HELLENIC REPUBLIC
National and Kapodistrian University of Athens
EST. 1837

School of Health Sciences

School of Medicine and Department of Pharmacy

Interdisciplinary M.Sc. course in

Nanomedicine

Academic year 2020-2021

Thesis Title: "*Functional nanoparticles for magnetic resonance C-Surgery tools"*

Τίτλος Διπλωματικής: *''Λειτουργικά νανοσωματίδια και οι εφαρμογές τους στην μαγνητική τομογραφία και χειρουργική ''*

Thesis Subject: In the area of functional nanoparticle for MRI and Image-guided surgery, their current medical applications, recent developments, challenges and future perspectives are discussed.

Candidate: Alexia-Christina Vakouftsi

Supervisors: Dionysios E. Mouzakis

Examination Committee: A. Pispas and A. Pippa

Date of Submission: 02/03/2022

Table of Contents

Abbreviations list

AIE: aggregation-induced emission

AKI: acute kidney injury

AF: atrial fibrillation

APCs :antigen-presenting cells

Au: gold

BRET: bioluminance resonance energy transfer

CA: contrast agent

CAS: computer-assisted surgery

CEST: Chemical exchange saturation transfer

CKD: chronic kidney disease

CT: computed tomography

DCs: dendritic cells

DLNs: draining lymph nodes

DLS: dynamic light scattering

DFRT: ferritin-loaded

DCNP: downconversion nanoparticle

ECM: extracellular matrix

EMEA: European Medicines Agency

ESIONs: extremely small-sized iron oxide nanoparticles

EPR: Enhanced permeability and retention

FDA: Food and Drug Administration

FRT: ferritin

FGS: fluorescence -guided surgery

FD-OCT: Fourier domain-optical coherence tomography

Gd: gadolinium

GNBS: gold nanobeacons

GFC: gel filtration chromatography

GPU: graphic processing unit

H&E: haematoxylin-eosin

ICG: Indocyanine green

IGS: imaging-guided surgery

IV: intravenous

LN: lymph node

MRI: magnetic resonance imaging

MMPs: metalloproteases

MRD: minimal residual disease

MPIO: micron-sized particles of iron oxide

MPS: monocyte phagocyte system

MLPS: magnetoliposomes

MONs: manganese oxide nanoparticles

MSCs: Multipotent mesenchymal stem cells

NWs: molecular weights

NM: nanomaterial

NMR: nuclear magnetic resonance

NP: nanoparticle

NTs: normal tissues

NIR: near-infrared

NIRF: near-infrared fluorescence

OCT: optical coherence tomography

PAI: Photoacoustic imaging

PAMAM: polyamidoamine

PDT: Photodynamic therapy

PTT: Photothermal therapy

PI: Postinjection

PS: Photosensitizer

PEG: polyethylene glycol

PDGF: platelet-derived growth factor

PET: Positron emission tomography

QDs: quantum dots

QY: quantum yield

RES: reticuloendothelial system

RF: radiofrequency

RGD: arginylglycylaspartic acid

SLN: Sentinel lymph node

SR: shift reagents

SPION: superparamagnetic iron oxide nanoparticle

SPIONs: superparamagnetic iron oxide nanoparticles

SPN: semiconducting nanoparticle

SPNs: Semiconducting polymer nanoparticles

SDT: sonodynamic therapy

SERS: surface enhanced Raman scattering

SERRS: surface enhanced resonance raman scattering

T/NT: tumor/normal tissue

TBR: tumor to background ratio

T: Tesla

tD: diffusion correlation time

U/S : ultrasound

USPION: ultra-small superparamagnetic iron oxide nanoparticles

VEGF: vascular endothelial growth factor

3D : three dimensional

Key words: Nanomedicine, functional nanoparticle, MRI, image-guided surgery

Λέξεις-κλειδιά: Νανοϊατρική, λειτουργικά νανοσωματίδια, μαγνητικη τομογραφια, εικονικά καθοδηγούμενη χειρουργικη

Abstract

The central purpose of this thesis is to provide a general overview of functional nanoparticles for MRI and image-guided surgery and their applications in the medical field. Nanoparticle-based contrast agents offer promising new platforms to increase the resolution and sensitivity of MRI by their enhanced accumulation at disease sites and their large surface area for additional modification with targeting ligands etc. The different types of contrast agents were discussed concurrently with any recent developments. This thesis reviews the ever-evolving interest in nanoparticle-based activatable MRI contrast agents responsive to various stimuli which enhances specificity and sensitivity. The principles of nanomaterials to surgical targets are reviewed, unlocking the advantages of nano-technology in image-guided surgery and multimodal image-guided surgery and assisted synergistic therapy. A pragmatic method to achieve intraoperative visualization with deep tissue penetration and high resolution is multimodal-imaging based on molecular imaging technologies. Furthermore, functional nanomaterials synergize different surgical procedures to eliminate residual lesions. Additionally, theragnostic nanomaterials with surgical applications were discussed. Finally, this thesis mentions the challenges and future perspectives to develop and translate functional nanoparticles for MRI and nanomaterials for image-guided surgery into clinical practice.

Περίληψη

Ο κεντρικός σκοπός αυτής της εργασίας είναι να παρέχει μια γενική επισκόπηση όσων αφορά την χρήση και εφαρμογή των λειτουργικών νανοσωματιδίων στην μαγνητική τομογραφία και της εικονικά καθοδηγούμενης χειρουργικής στον τομέα της ιατρικής. Τα νανοσωματιδιακά σκιαγραφικά μέσα προσφέρουν την δυνατότητα άριστης ανάλυσης και υψηλής ευαισθησίας μαγνητικής τομογραφίας μέσα από την ικανότητα τους να συσσωρεύονται στα παθολογικά σημεία καθώς και την ιδιότητα περεταίρω επεξεργασίας τους μέσω διαφόρων τεχνικών. Τα διάφορα είδη σκιαγραφικών ουσιών αναλύονται εκτενέστερα καθώς και οι πρόσφατες εξελίξεις στον συγκεκριμένο τομέα. Αυτή η διπλωματική αναλύει το συνεχώς αυξανόμενο ενδιαφέρον ως προς τα νανοσωματιδιακά

ενεργοποιούμενα σκιαγραφικά μέσα τα οποία ενεργοποιούνται έπειτα από συγκεκριμένα ερεθίσματα και προσφέρουν υψηλή ευαισθησία και εξειδίκευση . Οι αρχές της συσσώρευσης των νανοϋλικών στα χειρουργικά σημεία αναλύονται και αποτελούν προοίμιο για τα οφέλη της νανοϊατρικής στην εικονικά καθοδηγούμενη χειρουργική . Ένας ρεαλιστικός τρόπος για να παρέχουμε άρτια διεγχειρητική εικόνα και ικανοποιητική διείσδυση ιστών είναι η πολυτροπική απεικόνιση βασισμένη σε μοριακές απεικονιστικές τεχνολογίες. Επιπροσθέτως τα λειτουργικά νανοσωματιδιακά μπορούν να χρησιμοποιηθούν σε διαφόρου είδους χειρουργικές επεμβάσεις με στόχο την ολοκληρωτική εξαίρεση των παθολογικών εξεργασιών. Επιπλέον, ο σύγχρονος συνδυασμός της διάγνωσης και θεραπείας ταυτόχρονα και σε πρώτο χρόνο μέσω της χρήσης νανοσωματιδίων στον τομέα της χειρουργικής αναλύεται στα πλαίσια αυτής της διπλωματικής. Τελειώνοντας, αυτή η διπλωματική αναφέρει τις δυσκολίες και τις μελλοντικές προοπτικές όσον αφορά την ανάπτυξη , εξέλιξη και κλινική εφαρμογή των λειτουργικών νανοσωματιδίων στην μαγνητική τομογραφία και στην εικονικά καθοδηγούμενη χειρουργική .

A. Introduction

A1. Definition of Functional NPs for MRI

Magnetic resonance imaging (MRI) constitutes a non-invasive medical imaging method that utilizes protons, a strong magnetic field, and a radiofrequency pulse to provide anatomical images of soft tissues denoting the usage of MRI as a crucial diagnostic modality.[1,2] Even though MRI provides outstanding images of soft tissues it's the introduction of contrast agents that makes it possible to differentiate physiologic from pathological tissues by accelerating magnetic relaxation at specific areas of interest.[4] The distinctive attributes of nanoparticle-based contrast agents distinguish them as an attractive option for MRI. Firstly, nanoparticles possess the ability to carry multiple imaging moieties yielding signal amplification which allows for great imaging in a reduced contrast agent dose. Concurrently, reducing the cytotoxicity of the aforementioned contrast agent.[5] Secondly, due to their large surface area, nanoparticles can be customized with ancillary moieties to improve reactivity, targeting[6] or inserting a completely new functionality reentering them superior to their bulk counterparts. Furthermore, multimodal MRI contrast agents gaining traction because of their ability to display multiple features with a single contrast agent (CA) at the same site. Lastly, the enhanced permeability and retention (EPR) effect used by the nanoparticles to aggregate at a tumor site constitutes a significant signal/noise in tumors.[3]

A2. Image-Guided Surgery

Image-guided surgery employs pre-surgery images of the area of interest to accurately detect tumor margins, delineate metastatic lesions, and avoid damage to the surrounding healthy tissues. Regarding surgery and more precisely cancer resection, whenever R0 isn't achieved that equals increased recurrence rates and overall lower survival rates. [4]

B. Theory

B1.Basic Principles of Functional NP for MRI

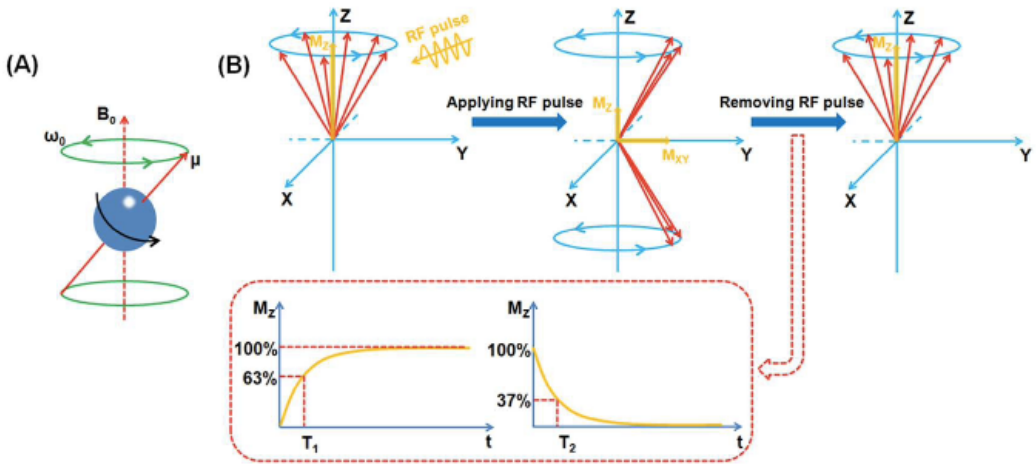

Fig. 1 Schematic illustration of the mechanisms of MRI. (A) Protons precess under external magnetic field B_0. (B) After the introduction of RF pulse, protons are excited, with relaxation occurring following removal of the RF pulse. And the graphical representation of T_1 relaxation and T_2 relaxation.

6

MRI detects protons of water molecules whose spin is aligned with the magnetic field. Subsequently, a radiofrequency pulse (RF) is applied, and protons absorb it and flip their spin. When the RF ceases the protons return to their previous spin and simultaneously release the energy in the form of radio waves which are captured by the receivers and translated into MRI images. T1, T2, r1, and r2 demonstrate vital parameters in our attempt to understand the inner workings of the MRI. Relaxation time which is divided into longitudinal (T1) and transverse (T2) is defined as the duration required by the protons to return to their original alignment within the magnetic field from the moment the RF pulse is stopped till their equilibrium. Relaxation time is tissue-dependent. As shown in Fig 1, T1 implies the time required for the magnetic vector to be restored to 63% percent of its original magnitude and T2 represents the time for the magnetization vector in the

perpendicular plane to the magnetic field to decrease to 37%. The contrast agents that are used in MRI usually impact both T1 and T2 but demonstrate more pronounced results in the T1 or T2 and are thus categorized as T1 contrast agents or T2 contrast agents. T1 CAs demonstrate a bright image due to their positive contrast enhancement and increase signal intensity in T1-weighted MRI, whereas T2 CAs provide a darker image due to their negative contrast enhancement and decreased signal intensity in T2-weighted MRI. Relaxation rate Ri= 1/Ti (s-1) , i=1 or 2 is used to measure contrast enhancement . ri (ri=Ri/c (mM-1s-1)), whereas c stands for the concentration of the CA. The r1/r2 determines the efficiency of the CA, higher ratios equal higher efficiency. The key to a more efficient selection of nanoparticles as MRI CA lies in the utilization of transition metal ions (Mn2+, Fe2+/Fe3+, Co2+, and Cu2+) and lanthanide metal ions (Eu3+, Gd3+, Ho3+, and Dy3+). To achieve high relaxation CAs the electron motion, nanostructure-dependent effect, and individualized relaxation mechanism must be taken into consideration. Contrast is enhanced when one tissue has more increased vascularity or higher affinity for the aforementioned contrast. Pathologic tissues, like tumors, are metabolically different from healthy ones and consequently can internalize the CA differently leading to a distinct MRI image. Currently, the majority of T1 CAs are paramagnetic complexes while T2 CAs are mainly superparamagnetic iron oxides. In summary, MRI is one of the most important diagnostic tools in medicine but the low sensitivity due to the FDA-approved magnetic field of 3 Tesla remains challenging leaving the manipulation of the physiochemical properties of CAs our main chance of improving MRI.[6]

B2. Enhanced accumulation of NPs at surgical sites

Table 1. Targeting systems for enhanced accumulation of nanomaterials in surgical targets.

Targeting system	Specific targets	NMs	Applications	Refs.
Passive targeting via EPR effect	–	PDFT1032	LN mapping and biopsy, osteosarcoma imaging and IGS	[31]
	–	SNPs	LN mapping	[32]
	–	PDI NPs	LN mapping and biopsy, glioblastoma imaging and PTT guidance	[33]
	–	AGL AIE dots	Peritoneal carcinomatosis imaging and IGS	[34]
	–	HLZ-BTED dots	Breast tumor imaging and visualizing tumor feeding blood vessels	[35]
	–	L897 NPs	LN and glioblastoma imaging	[36]
	–	BPN-BBTD NPs	Bladder tumor imaging and PTT guidance	[37]
Active targeting via ligands				
Peptide	FSH_β receptor	DCNP-L_1-FSH_β	Ovarian cancer imaging and IGS	[38]
	Integrin $\alpha_v\beta_3$	IR-BEMC6P@RGD	Gastroenteropancreatic neuroendocrine tumor imaging and IGS	[39]
		T-TTD dots[a)]	Cholangiocarcinoma imaging and PDT guidance	[40]
		T-TPETS nanodots[b)]	Hepatocellular carcinoma, imaging and PDT guidance	[41]
		^{68}Ga-SCH2	Glioblastoma imaging and IGS	[42]
	SSTR	IR-BEMC6P@TATE	Gastroenteropancreatic neuroendocrine tumor imaging and IGS	[39]
	EGFRvIII	AuP-FAL	Glioblastoma imaging and IGS	[43]
	EphA2 protein	DTE-TPECM NPs	Breast tumor imaging, IGS and PDT	[44]
Vitamin	Folate receptor	PFH/DOX@PLGA/Fe_3O_4-FA	Hepatoma imaging and synergized HIFU with chemotherapy	[45]
Antibody	CD47 CA9	s420-CD47 s420-CA9	Bladder tumor imaging and IGS	[46]
Aptamer	Endoglin (CD105)	Den-Apt1	Hepatic tumor imaging and IGS	[47]
Protein	PSMA receptor	AuNP5kPEG-PSMA-1-Pc4	Prostate cancer imaging and PDT guidance	[48]

[a)]T-TTD: a targeted red emissive aggregation-induced emission photosensitizer conjugated with thiolated cRGD (TTD: 2-(2,6-bis((E)-4-(phenyl(4′-(1,2,2-triphenylvinyl)-[1,1′-biphenyl]-4-yl)amino)styryl)-4H-pyran-4-ylidene)malononitrile); [b)]T-TPETS: a targeted red emissive aggregation-induced emission photosensitizer conjugated with thiolated cRGD (TPETS: a tetraphenylene derivative).

4

NP systems are constructed taking into consideration the pathophysiology of tumors along with the physiochemical characteristics of NMs expressing their tumor targeting abilities and highlighting their potential role and application in cancer diagnosis, treatment, and oncological surgery[7,6]. The main targeting approaches of NPs are passive and active targeting (Table 1). Passive targeting utilizes the EPR effect and the size of the particular NP[9,10]. Tumor sites experience augmented and defective angiogenesis along with defective lymphatic drainage. The increased and dysfunctional angiogenesis results in increased permeability of vessels and ultimately easier access of the NPs into tumor sites[11,12]. Smaller NP ~10 nm can travel freely through the circulatory system and is excreted into the urine by the kidneys. On the other hand, larger NPs ~100nm are metabolized by the RES, liver, and spleen[13,14]. NP hydrophilicity through the EPR effect can enhance their delivery rate and reduce their LN retention[15]. A combination of positive charge and decreased NP size leads to better targeting ability with antigen-presenting cells (APS) such as dendritic cells (DCs) and macrophages[16]. Furthermore, neutral or negative surface charges in hydrophilic stealth NPs can diffuse into the deeper tissue matrix. In active targeting NPs combined with a variety of ligands and receptors in tumors[8,17] and can be further subdivided according to

the properties and functions of the conjugated molecules. Has been established that specific tumor cells and tumor stem cell targets express high specificity to certain cancer types[18,19]. Nowadays, active and passive targeting methods have been widely exploited to deliver NPs with high sensitivity and specificity at tumor sites. The state of angiogenesis and vascularization in solid tumors determines the ability of the NP system through the EPR effect to accumulate into the area of interest and for us to obtain tissue-specific imaging. For the EPR effect to take place nanocarrier size should be a minimum of 50 nm and possess long blood circulating time. This can be achieved by constructing nanocarriers of the correct size and functionalizing them with water-soluble molecules to avoid rapid renal clearance. Chan et al. investigated the effects of NP size and surface chemical profile on passive targeting in tumors in vivo and concluded that the smaller NPs tended to diffuse throughout the tumor compared to the larger ones that stayed in the vasculature. Even though an abnormal vasculature promotes the EPR effect, the tumor architecture comprises a heterogenous distribution that can inhibit the accumulation of NPs. The tumor interstitium consists of a fluid and a matrix part. The fluid part comprises mainly proteins (cytokines, growth factors, and metalloproteases) and has acidic pH values and low oxygen levels resulting in an away movement of the fluid from the central region of the tumor and consequently in a decreased ability of the NP to reach the inner tumor mass. The extracellular matrix results from a complex assembly of collagen, glycosaminoglycans, proteoglycans, and cancer-associated fibroblasts. The aforementioned work provided insight to better engineer NP for cancer therapeutics. NIR fluorescent dyes were manufactured and conjugated with specific tumor-targeted moieties in an attempt to reduce their delivery to healthy tissues and enable them to target only the pathologic ones and ensure more precise tumor detection by eliminating the background signal associated with nonspecific binding through active targeting. Concluding both active and passive targeting can be used to ameliorate cancer through the suitable design of organic or inorganic nano-therapeutic agents in size, shape, composition, surface charge, and functionalization. Opsonization plays an important role in the clearance of NPs leading to the surface coating of NPs with hydrophilic polymers such as polyethylene glycol (PEG) to improve the stability of the NP and ensure their increased circulation time by avoiding clearance through the RES. New cell-membrane camouflaged NPs have been proposed as nature-inspired biomimetic delivery systems for cancer treatment due to their great

biocompatibility, no immunogenicity, and prolonged circulation lifetime. Indeed, the development of intelligent nanosystems can lead to the effective internalization of NPs into cancer cells while taking into consideration the tumors microenvironment (low pH values or elevated expression levels of tumor-associated enzymes) and the external stimuli (ultrasound, light, magnetic field) after their extravasation.[4]

The ideal outcome of any successful oncological operation is to achieve complete resection of the tumor with minimal damage to normal tissues (NTs). In an attempt to actualize the aforementioned goal intraoperative imaging with visualization and navigation systems for real-time surgery was employed. The features that these intraoperative agents should possess are good biocompatibility, deep tissue penetration, no long-term cytotoxicity and offer the surgeon optimal time to perform the required procedure[18]. The goal is to develop novel optical probes with high quantum yield (QY) and long tumor retention to achieve precise and effective IGS. The aggregation-induced emission (AIE) describes how certain organic compounds have a photophysical effect in which the luminesce of aggregates is stronger than that in a dispersed state[20]. Therefore, novel probes with high QY can be designed using the aforementioned phenomenon. NP delivery systems encapsulating AIE luminogens experience improved brightness in solid or aggregated conditions.[21, 24] Ni and co-workers developed afterglow luminescent AIE NPs (AGL AIE dots, Figure 2a) with an appropriate window for IGS.[25] An IV injection of the AGL AIE dots offered a high T/NT and the visualization of sub-millimeter-sized tumors. Targeted image guided theranostic for cholangiocarcinoma and hepatocellular carcinoma was achieved through the development of two different integrins αvβ3 targeted AIE dots (Figure 2b,c)[22,23]. Furthermore, NIR-II fluorophores (Figure 2d) and PA nanoprobes (Figure 2e) through the AIE phenomenon can achieve high QY, T/NT, and ultrabright signals.[26,27,28,29,30,31]

Recent studies on NIR-II fluorescence-guided surgery (FGS) offered considerable advantages in a high T/NT ratio to facilitate tumor resection[32,33,34]. Wang et al. as shown in (Figure 3a) constructed an in vivo assembling downconversion NP (DCNP) modified with DNA (L1) and follicle-stimulating hormone (FSHβ) peptide (called DCNP-L1-FSHβ) which is used to effectively resect abdominal ovarian micro metastasis smaller than 1 mm and guide resection with NIR-II imaging[35]. Two sequential IV injections with the DCNP-L1-FSHβ were performed and showed retention in tumor higher T/NT from 20 to 26h with an approximately 6-hour surgical window (Figure 3b–e). The successful resection was

confirmed with Haematoxylin-eosin (H&E) staining (Figure 3f). Dai's team used fluorophore IRT based on donor-accepter-donor (D-A-D) structure and conjugated to a novel peptide CP and manufactured a NIR-II fluorescence probe (CP-IRT) with enhanced T/NT signal. Additionally, the majority of CP-IRT probes were renally excreted within 6 h[36].

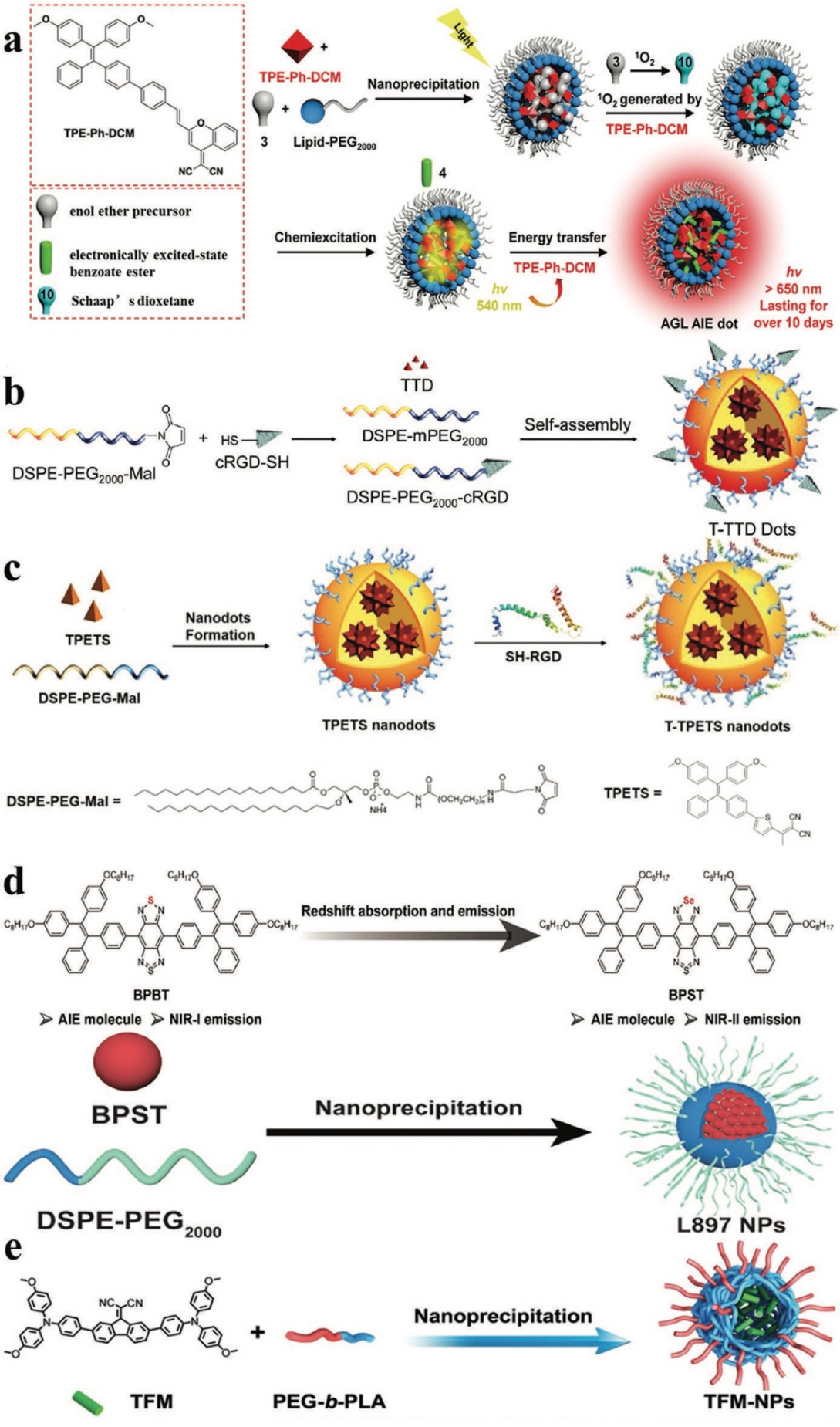
a
TPE-Ph-DCM
enol ether precursor
electronically excited-state benzoate ester
Schaap' s dioxetane
TPE-Ph-DCM
Lipid-PEG2000
Nanoprecipitation
Light
3
1O2
10
1O2 generated by TPE-Ph-DCM
4
Chemiexcitation
Energy transfer
TPE-Ph-DCM
hv
540 nm
AGL AIE dot
hv
> 650 nm
Lasting for over 10 days
b
TTD
DSPE-PEG2000-Mal
HS
cRGD-SH
DSPE-mPEG2000
DSPE-PEG2000-cRGD
Self-assembly
T-TTD Dots
c
TPETS
DSPE-PEG-Mal
Nanodots Formation
TPETS nanodots
SH-RGD
T-TPETS nanodots
DSPE-PEG-Mal =
TPETS =
d
Redshift absorption and emission
BPBT
AIE molecule
NIR-I emission
BPST
AIE molecule
NIR-II emission
BPST
DSPE-PEG2000
Nanoprecipitation
L897 NPs
e
Nanoprecipitation
TFM
PEG-b-PLA
TFM-NPs

Figure 2. Image-guided theranostics via AIE NPs. a) The principle of AGL AIE dots. b) Image-guided PDT of cholangiocarcinoma via T-TTD dots with one-step formulation. c) T-TPETS nanodot formation and surface modification to perform image-guided PDT for hepatocellular carcinoma. d) Design of structural formulas for NIR-II fluorescent imaging. e) PA imaging-guided PTT via a anovel aggregation-induced emission luminogen..[39]

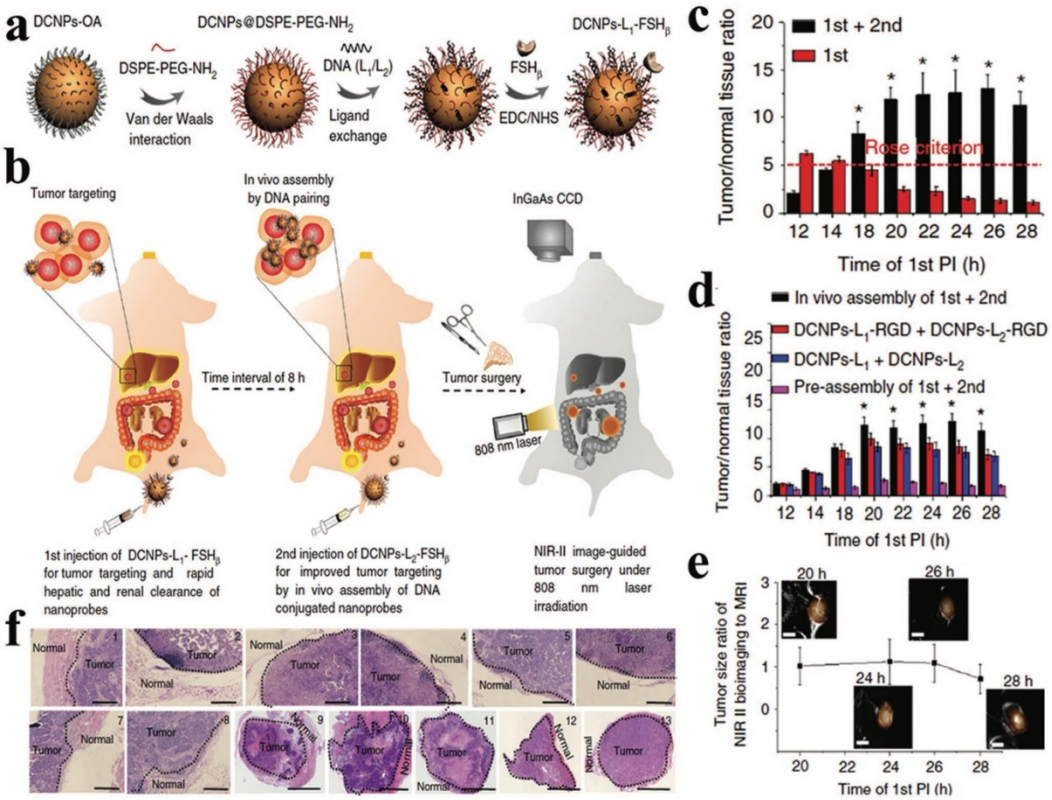

Figure 3. The stepwise development of DCNP-L1-FSHβ as NIR-II fluorescence probe for cancer detection. a) Schematic representation of DNA and FSHβ modified DCNPs. b) The assembly of DCNP-L1-FSHβ (first injection) and DCNP-L2-FSHβ (second injection) which showed increased tumor targeting and rapid hepatorenal clearance after 2 sequential injections. c) T/N ratio in 1st and the 2-stage process. d) T/N ratio of the pictured groups. e) MRI and NIR-II fluorescence correlation regarding the tumor size ratio. f) H&E staining results of tumor margins.[40]

C. Methods

C1. Search strategy

A systematic literature search for this review was carried out using the electronic database PubMed. The search strategy for each of the databases is depicted in Table 1.

Table 1. Literature search strategy

keywords	Citations retrieved (14.06.2021)	Studies selected after screening of title and abstract
Functional Nanoparticles + MRI	5,530	87
Nanomaterial + image-guided surgery	281	38
Theranostic nanomaterial + surgery	703	64
Nanoparticle + MRI contrast agents	6,315	128
Nanoparticle-based MRI contrast agents + surgery	14	9

In addition, the reference sections of the retrieved studies were hand-searched for relevant studies.

C2. Selection criteria

For the identification of relevant papers, the following criteria were applied.

Inclusion criteria:

- Case reports, clinical trials and reviews.
- The paper had to include data regarding image-guided surgery and MRI contrast agents
- The paper had to include data regarding nanomedicine, nanoparticles, MRI and surgery.
- Language: English

Exclusion criteria:

- Newspaper articles, conferences abstracts and letters
- Publications with only theoretical approach

D. Results

D1. Different types of Contrast Agents

The basis of conventional MRI lies in detecting signals from protons. Relaxation time which is tissue-dependent can be longitudinal (T1) or transverse (T2). A variety of contrast agents (CAs) have been developed to improve image contrast. Contrast agents can be classified according to the chemical exchange saturation (CEST) effect and the modification of tissue relaxation times (T1, T2).

D1.1 T_1

GADOLINIUM AND CHELATES

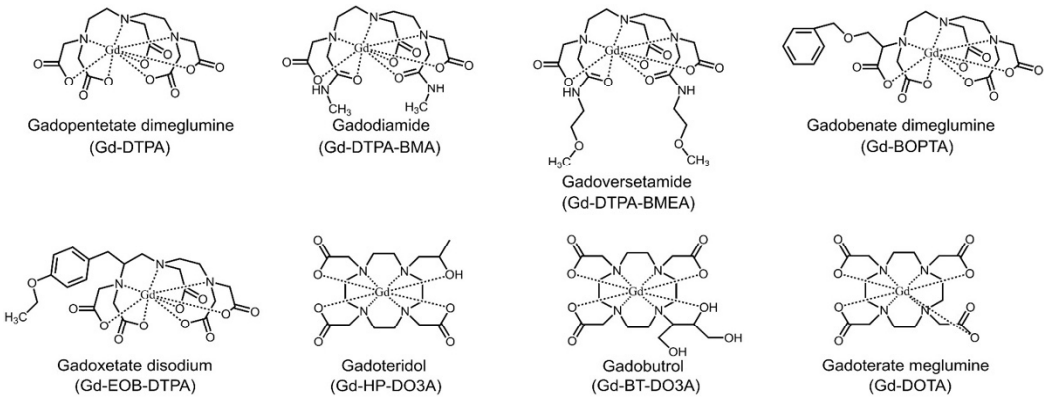

Fig.10 Chemical structure of currently marketed gadolinium-based MRI CAs. [38]

Gadolinium a metal ion constitutes the gold standard in clinical MRI due to an electron spin of 7/2.fig 10[38] Nowadays, we know that free Gd ions are cytotoxic due to their retention in the spleen, liver, and bone so a chelating process was introduced to counteract this cytotoxicity. Frequently used and widely known chelating compounds are dipyridoxyl-

diphosphate (DPDP), 1,4,7,10- tetraazacyclo-dodecane-1,4,7,10-tetraacetic acid (DOTA) and diethylene-triamine-pentaacetic acid (DTPA)[17]. Despite the fact that a chelating process reentered Gd as a safe option for a contrast agent, the World Health Organization (WHO) deemed Gd contrast agents contraindicated in people with CKD or AKI due to higher instances of hepatorenal syndrome in neonates and the development of nephrogenic systemic fibrosis. Gd-based contrast agents possess low molecular weight, are mainly extracellular, and experience rapid extravasation from the vascular space to the interstitium. Following, an IV injection the Gd-based contrast agent has a half-life of distribution of ~5min and in its majority excreted by the kidney in ~80 min[17]. A worth noticing and readily available class of MRI contrast agents employs Gd chelates hydrophilic macromolecule nanoparticle CAs with the use of dextrans, polylysine derivatives, dendrimers, polymeric Gd complexes, and Gd-chelate latex nanoparticles, liposomes, and micelles[41,20, 23,24,26,43, 45,46,47]. The PAMAM dendrimers due to their unique biological and physiochemical characteristics demonstrate the ability to process multiple free amino groups on their surface manufacturing an excellent template to synthesize Gd-chelate grafted nanoparticles.[42,44,30]. Cheng and co-workers have developed a concrete approach to synthesizing nanometer-sized dendrimer nanoclusters.[44] Huang and co-authors have developed gadolinium-conjugated PAMAM dendrimer nanoclusters as T1-weighted MRI contrast agents. Conjugating cancer-targeting ligands such as folic acid with the Gd-conjugated dendrimer nanoclusters could provide a stepping stone to higher sensitivity and specificity MRI cancer detection.[30] In an attempt to decrease cytotoxicity the Gd PAMAM dendrimer clusters are crosslinked through biodegradable polydisulfide linkages to larger nanocluster. Consequently, they experience high T1 relaxivity and extended circulation time. Subsequently, they are degraded to smaller products and undergo renal excretion so no long-term macromolecular particle retention is demonstrated and a size controllable and biodegradable dendrimer nanocluster with vast clinical applications is designed. Liu and co-authors, focusing on early detection of HCC manufactured a multifunctional polymeric nanoparticle contrast agent (Anti-VEGF PLA-PEG-PLL-Gd NP) concomitantly modified with Gd-DTPA and anti-(VEGF) antibody to deliver Gd-DTPA to the tumor. All in all, the Anti-VEGF PLA-PEG-PLL-Gd NPs had great tumor selectivity, good biocompatibility, and a high T1 relaxation time making them a potential lifesaving diagnostic tool.

Gd chelates to increase their function, blood-brain barrier permeability, and overall intrinsic cell uptake have been conjugated with various moieties. For instance, the conjugation of Gd-DTPA to albumin led to longer relaxation times and enhanced signals in the heart and liver. The encapsulation or conjugation of Gd chelated to macromolecules such as liposomes, dendrimers and micelles offers an increased stability and circulation time. Fluorescent labeling and cellular entry of plasmid DNA (pDNA) were achieved through the Gd-liposome complex. Gd-DOTA- phosphatidylethanolamine N-methyltransferase (Gd-DOTA-Chol 1, MAGfect) achieved in vitro cell labeling.[48] In vivo xenograft tumors were examined using a bimodal (2-{4,7-bis-carboxymethyl-10-[(N,N-distearylamidomethyl-N'-amidomythyl)−1,4,7,10-tetraazacyclododec-1-yl]}(Gd-DOTA-DSA) Gd liposome and coating it with PEG. The complex demonstrated MR and fluorescence imaging and the uptake of the complex by the cells resulted in increased T1 relaxation time.[49] Imaging of atherosclerotic plaques achieved with the use of paramagnetic Gd-chelate linked with liposomes enriched with phosphatidylserine PS (Gd-PS) to target macrophages which play a major role in the atherosclerosis process.[50] Concluding, the extended circulation time of Gd liposomes in tumors stipulates their use as therapeutic agents in cancer treatment by carrying therapeutic drugs or genes.

It has been reported and verified by multiple researchers that Gd oxide NP especially ultra-small Gd2O3 NP exhibit increased T1 relaxation times compared to other Gd complexes. The aforementioned statement can be attributed to an optimal surface-to-volume ratio of small nanoparticles.[51] Furthermore, in 2007, Fortin et al coated with polyethyleneglycol (PEG) and diethylene glycol (DEG) ultra-small Gd203 NPs and concluded that the PEG-coated complex exhibited higher relaxivities and enhanced signal intensities.[52] Wu et al. manufactured folic acid (FA)- conjugated, bovine serum albumin (BSA)-coated Gd2O3 nanoparticles (FA-Gd2O3@BSA) which exhibited increased r1 values (10.8 mM-1s-1) in comparison to Magnevist (3.8 mM-1s-1) and were stable in serum with good biocompatibility.[53] Gao et al. reported a r1 relaxivity of 45.08 mM-1s-1 based on ultra-small Gd2O3 NP by utilizing worm-like interior channels of mesoporous silica nanospheres synthesizing the Gd2O3@MSN nano-composites.[54] Roux and co-workers highlighted the enhanced MRI performance of small NP by synthesizing organic dyes functionalized ultra-small Gd2O3 nanoparticles embedded in a polysiloxane shell for MRI and fluorescence imaging.[52]

Bares meaning to emphasize that multifunctional nanosystems based on Gd2O3 nanoparticles were designed for theragnostic purposes. Zhao et al. designed rare-earth-doped Gd2O3 hollow nanospheres using hydrothermal carbon spheres and loaded ibuprofen as the model drug for concomitantly T1-weighted MRI, UCL imaging, and drug delivery. Zhao et al. reported great drug absorption, storage, and release.[55] Lastly, gadolinium-based upconversion NP because of its substantial magnetic and optical properties can be used for multifunctional imaging, including T1-weighted MR and UCL.[58,59,60,61,62,63,64,65] Song et al. designed ultra-small and hexagonal NaGdF4-based upconversion NP and Veggel et al. a series of ultra-small NaGdF4-based upconversion NP that serves the aforementioned goal as dual-modal imaging.[56]

QUANTUM DOTS

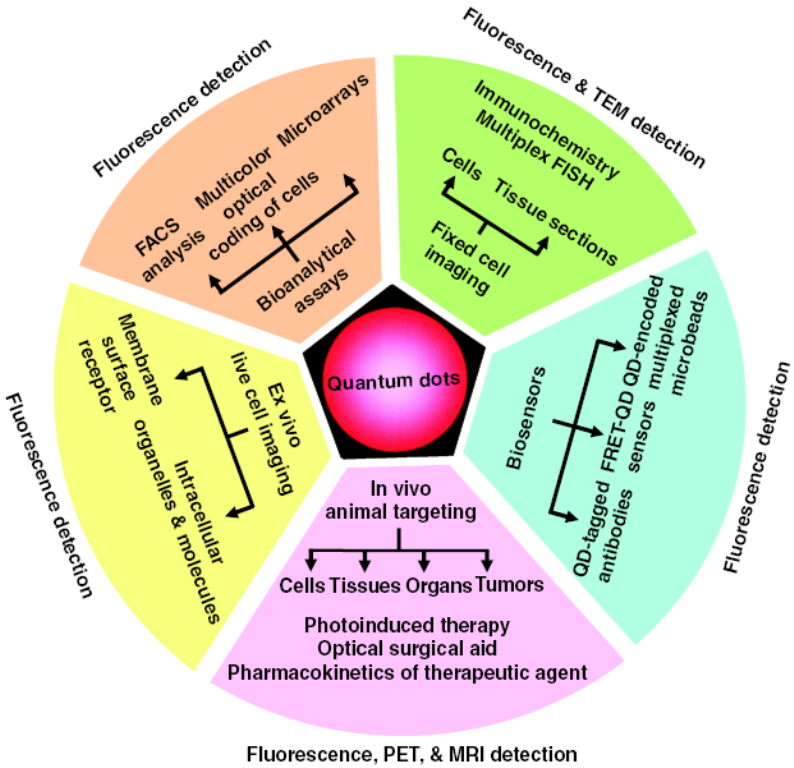

Fig.11 Quantum dots applications in bioimaging[7]

Regarding biomedical research, imaging, and clinical applications quantum dots are extensively utilized due to their unique optical properties (broad absorption spectra, size dependant emission) as semiconductor nanocrystals with fluorophores. Fig 11[66] Conjugation of Gd-chelates with QDs, magnetic NPs with the heterocrystalline growth,

core/shell formation of QDs, and doping with paramagnetic metal ions like Gd3+ to QDs lead to the manufacturing of QD-based multimodal imaging probes. For instance, a bimodal nanosystem constructed of hydrophilic CdTe QDs conjugated to Gd-1,4,7,10-tetraazacyclododecane-1,4,7-triacetate (DO3A) monoamide chelates, Gd-1,4,7,10-tetraazacyclododecane-1,4,7-tris- acetate-10-succinimidyl acetate (DO3A-NHS) designed to highlight the usage of QDs as bimodal probes and combine the advantages of fluorescence and MR imaging methods.[42] A bimodal probe of fluorescence imaging and MRI bares the complimentary effect of ameliorating the limitation of MRI to depict molecular/cellular biochemical events. Subsequently, high longitudinal relaxivities can be achieved by bimodal nanoprobes with the fine-tuning of the ratio of the QDs and Gd-chelates via fluorescence characteristics, correlation spectroscopy analysis, and probe stability. For example, the surface of core-multishell CdSe/CdS/ZnS QDs was grafted with thiol-functionalized Gd-chelates and resulted in a nanoprobe with astonishingly high T1 relaxivity and photoluminescence.[43]

Consequently, a CdSe/ZnS core/shell QDs coated with paramagnetic PEGylated lipids, Gd-DTPA-bis(stearyl amide) bimodal photoluminesce-MRI imaging probe with great biocompatibility were developed.[44] In 2014, ultra-small NaGdF4 nanodots were manufactured by pyrolysis. This complex demonstrated greater MR performance ~2.4 times as a contrast agent compared to the clinical standard Magnevist and was excreted through the kidneys.[46] Lastly, a bimodal optical and MR probe for imaging cell death and platelet activation was actualized by the use of the annexin A5-functionalized QDs with biotinylated Gd-DTPA.[45,47]

MANGANESE

The conjugation of Mn ions with chelates such as DPDP, DTPA, and porphyrin rings leads to the formation of small molecules. Small molecule CAs and nanoparticulate CAs are the two main categories of Mn-based paramagnetic nanoparticles. Mn nanoparticulate systems can be applied to neuroimaging due to the ability of Mn ions to enter cells via calcium channels. Modification of Mn chelates with their absorption into lipid bilayers leads to the formation of nanoparticulate systems such as MnO, MnO2, and Mn3O4. [49] In 1997 FDA approved the utilization of Teslacan®, St Louis MO, USA an Mn- based CA for liver imaging. In 2012 the

EMA prohibited marketing authorization in the EU due to their well-known side effect profile.[48]

PARAMAGNETIC MANGANESE DENDRIMERS

Figure 6.

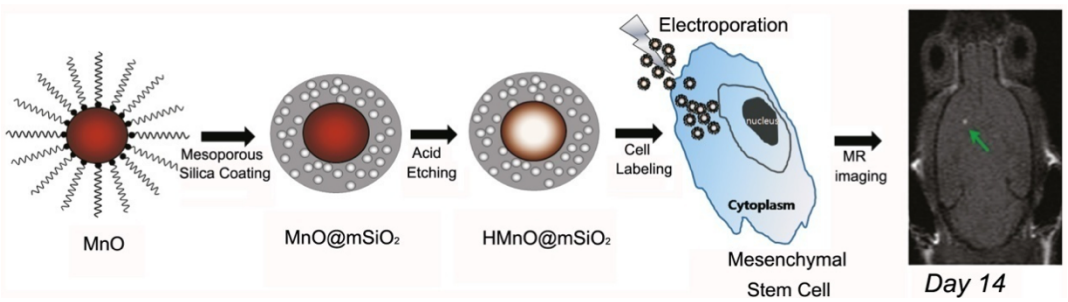

Schematic illustration of the synthesis of HMnO@mSiO$_2$ nanoparticles and labeling of mesenchymal stem cells (MSCs) and *in vivo* magnetic resonance imaging (MRI) of MSCs transplanted mouse .

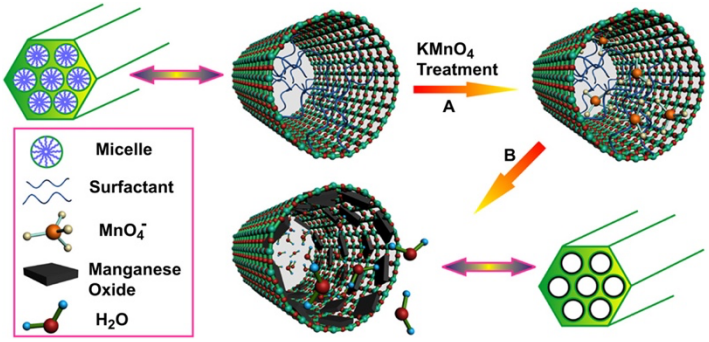

Figure 7. Schematic representation for the preparation of manganese oxide/mesoporous silica nanoparticles (MSNs)-based T_1-weighted MRI contrast agents .

Due to demonstrated nephrogenic systemic fibrosis (NSF) by Gd-based contrast agents, manganese ions emerged as an attractive alternative MRI contrast agent. Mn+2 at higher magnetic fields displays higher relaxivities than Gd.[50] To synthesize effective Mn-based contrast agents nanoparticulate systems such as MnO, Mn3O4, Mn3O4@SiO2, MnO@mesoporous SiO2, and hollow MnO nanoparticle should be employed. The main issue lies in the accessibility of the Mn paramagnetic centers to water molecules.[51,53, 55, 57]

Kim and co-authors introduced HMnO@mSiO2 as depicted in Fig.6 which contains a hollow Mn core structure and a coating consisting of mesoporous silica. The porous coating in combination with the increased surface-area-to-volume ratio derived from the new structure resulted in higher water accessibility to the manganese core and overall enhanced T1-weighted contrast. The HMnO@mSiO2 NPs displayed higher r1 compared to the existing Mn0 NP-based contrast agents.[56] Consequently, in vivo and in vitro experiments promise clinical applications as a T1-weighted MRI cell tracking for the HMnO@mSiO2 nanoparticles. Chen and co-authors presented a non-toxic manganese oxide/mesoporous silica nanoparticle (MSN)-based T1-weighted MRI contrast agents by means of oxidation/reduction reaction in-situ in mesopores followed by hydrogen reduction. This endeavor resulted in a nanoparticulate system with comparable imaging performance to commercial Gd-based agents (as shown in Figure 7).[54] The major upside in the nanoparticulate was the large surface-to-volume ratio and the high water-accessibility to manganese paramagnetic centers that were guaranteed by the highly dispersed MnO nanoparticles in the intelligent mesopore system. Mn ions employed as T1 MRI contrast agents to map cellular activity experience some drawbacks including cardiac toxicity. In an attempt to overcome said drawbacks inorganic manganese oxide nanoparticles (MONs) were designed. Spherical MnO nanoparticles display precise anatomical features of brain structures and are employed as T1- weighted MRI CAs.

Recently MONs with a range of morphology and different sizes have been reported concluding that by controlling the size and shape of the NP, modulation of their relaxivities is possible. Park et al. designed a lamellar structured ultrathin MnO nanoplate by employing 2,3-dihydroxy naphthalene (2,3-DHN) which subsequently promoted two-dimensional growth by acting as a structure-directing agent and as a solid binding surfactant. The nanoplate had an r1 of 5.5 mM−1 s−1 which at the time reported was the highest r1 value among MON-based MRI contrast agents. MRI results showed enhanced contrast in T1 in blood vessels, gallbladder, liver, and brain. HMnO@mSiO2 an HMnO encapsulated with a mesoporous silica shell possesses good opportunities for stem cell tracking. MRI with the aforementioned complex was carried out for in vivo cell tracking and labeled MSCs were serially followed for 14 days. Mice that were transplanted with the HMnO@mSiO2-labeled MSCs showed hyperintense regions in MRI even after 14 days.[60] In conclusion, hollow NPs

constitute attractive options for delivering therapeutic drug molecules because of their large surface area and their ability to hold big payloads.

IRON

ULTRASMALL IRON OXIDE NANOPARTICLES

Nanosystems	Size (nm)	r_1 ($mM^{-1}s^{-1}$)	r_2 ($mM^{-1}s^{-1}$)	r_2/r_1	Magnetic field (T)	Theranostic modes	*In vivo* (Y/N)
Fe_3O_4	5/9/12/16/22	-	-	-	-	-	N
Fe_3O_4	4/6/9/12	-	-	-	-	MRI	N
Fe_3O_4	6/12	-	-	-	-	-	N
POPEG-Fe_3O_4	2.2/3	4.78/4.77	17.5/29.2	3.67/6.12	1.5	MRI	Y
γ-Fe_2O_3-Citrate	5	20.76	51.02	2.46	-	MRI	N
PEG-Fe_3O_4	4	7.3	17.52	2.4	1.41	MRI	N
Fe_3O_4	4	5.991	15.534	2.59	0.5	MRI	N
$ZnFe_2O_4$	4	7.928	14.642	1.85	0.5	MRI	N
$NiFe_2O_4$	5	6.85	12.921	1.89	0.5	MRI	N
GSH-Fe_3O_4	3.72 ± 0.12	3.63	8.28	2.28	3	MRI	Y
RGD-PEG-Fe_3O_4	2.7	1.37	-	-	0.5	MRI	Y
MDBC-Fe_3O_4	3.4	4.75	21.73	4.7	1.41	MRI	Y
Cat-MDBC-Fe_3O_4	3.4 ± 1.8	6.8	37.1	5.5	1.41	MRI	N
PEG-Fe_3O_4	1.7	4.46	15.01	3.4	1.5	MRI	N
Fe_3O_4	1.9	1.415	2.87	2.03	7	MRI	N
Fe_3O_4	5.1 ± 0.5	5	182	36.4	3	MRI	N
^{68}Ga-C-Fe_3O_4	2.2 ± 0.2	5.7	22.2	3.89	1.5	MRI/PET	Y
PEG-Fe_3O_4	5.4	19.7	39.5	2	1.5	T_1-/T_2-MRI	N
PEG-BP-Fe_3O_4	5.5 ± 0.7	9.5	28.2	2.97	3	MRI/SPECT	Y
Fe_3O_4 nanotubes	9.7 ± 0.5	5.23	89.68	17.2	3	T_1-/T_2-MRI	Y
Gd-Fe_3O_4	4.8	7.85	41.14	5.24	7	MRI	Y
AuNR@PPy@Fe_xO	52	1.07	5.1	4.8	0.5	MRI/PTT	N

Table 2: T1-weighted MR performance of ultra-small iron oxide nanoparticles. [67]

Developing ultra-small iron oxide nanoparticles for T1-weighted MRI has attracted the interest of many researchers in recent years. Sun, Hyeon, and Cheon's manufactured monodisperse ultra-small Fe3O4 nanoparticles with T1-weighted MRI performance.[61,

[63,64,65] Weller et al. created PEG-coated ultra- small Fe3O4 nanoparticles (4nm diameter) taking advantage of the biocompatibility of PEG molecules to enhance the water solubility of Fe3O4 NPs and their high stability together with their low nonspecific phagocytosis by macrophages.[68] The aforementioned formulation exhibited high T1-weighted MRI performance. In 2007, Muller et al. designed ultra-small γ-Fe2O3 nanoparticles (5nm in diameter) with a very narrow distribution, strong saturation magnetization, and great stability in water at physiologic pH. The formulation exhibited through T1-weighted MRI the r1 value of 20.76 mM-1s-1.[69] Oh, et al. coated ultra-small Fe3O4 NPs with multi-dentate block-copolymer (MDBC) and reported great colloidal stability and high r1 relaxivity (4.75 mM-1s-1)[70]. The utilization of aqueous colloids as effective CAs for vascular T1-weighted MRI gained traction after ultra-small Fe3O4 NPs were stabilized by multi-dentate block copolymer with a multitude of catechol groups and demonstrated enhancement in T1-weighted MRI and great colloid stability[71].

It is of utmost importance to note the design of thermo-sensitive polymer attached with Fe3O4 nano- thermometers as T1-weighted CAs at a standard field MRI resulting in higher r1 at lower temperatures.[72]

The theory that hydrodynamic diameter has a paramount effect on iron oxide-based T1 MRI CA concomitantly with the utilization of PEGs with augmented molecular weights in an effort to minimize particle aggregation was tested by Tromsdorf et al. They displayed a monodisperse 4- and 6nm-sized iron oxide NPs with PO_4 functionalized with PEG of different chain lengths. Then, four kinds of PEG molecules with increasingly higher molecular weights utilized. Utilizing the method of dynamic light scattering in tandem with gel filtration chromatography, reported that PEGs with bigger MWs resulted in smaller hydrodynamic diameter. Finally, Fe2O3 NPs coated with PEG-1100 demonstrated r2/r1 value (equal to 2.4) together with r1 value (equal to 7.3 mM-1 s-1). Kim et al. synthesized extremely small-sized iron oxide nanoparticles (ESIONs) (1.5–3.7nm) with the method of thermal decomposition utilizing iron–oleate complexes. The aforementioned complex displayed very low magnetization due to the spin canting effect[48,56] . This low magnetization of ESIONs leads to an r2 (17.5 mM−1 s−1) and a decreased r2 /r1 ratio (3.67). Lastly, utilizing PEG-stabilized ESIONs the vasculature visualization via T1-weighted MRI was established.[59]

D1.2.T_2

Iron Oxide

Taking into consideration the core size of the NPs, we can subdivide this class of nanoparticles into superparamagnetic or ferromagnetic and utilized as T2 contrast agents for a long time. Maghemite and magnetite are commercially used compounds for biomedical imaging. These two express favorable characteristics such as chemical stability under physiologic conditions, reduced toxicity, and high magnetic moments.[50]

Starch, poly(ethylene glycol) (PEG), sulphonated styrene-divinyl-benzene, dextran, albumin, chitosan, alginate, organic siloxane, poly(ethylene imine and bioactive molecules like liposomes employed to stabilize the iron oxide NPs by encapsulated into or anchored onto the iron oxide surface.[51] Size is one of the most important contributing factors in the biological distribution of NPs. Subsequently, we encounter USPIONs with a diameter < 50 nm, SPIONs with a diameter in the hundreds, and MPIO diameter > 1 μm.[53] The latter is administered orally and the rest IV enhancing their advancement through the gastrointestinal tract.[54] The SPION Gastromark® for oral administration is FDA, EMEA approved and on the market and used for gastrointestinal bowel marking.[7] The value of r2 is influenced by the type of coating and its thickness, the most widely used are dextran and carboxy-dextran for SPIONs.[55] The biodistribution in conjugation with the pharmacokinetics of the aforementioned compounds are guided by their size and NPs and those with a size of 5.5 are renally excreted.

Relaxivities of ~1,000,000 mM-1·s-1 are required to reach acceptable contrast-to-noise ratios at the commercial field strength, therefore targeting mechanisms has to be employed.[56]

Active targeting strategies with ligands that are recognized by molecular signatures of the diseased cells have been used to increase the sensitivity of SPIONs. SPIONs are rapidly phagocytosed by macrophages after IV administration 80% of the dose is found within the liver and 5%–10% within the spleen, with a plasma half-life of 10 min and consequently decreases the signal in the liver and spleen.[57] Research has shown that malignant tumors lack Kupffer cells so utilizing SPIONs in the visualization of these tumors results in a powerful contrast between normal and abnormal tissue on T2-weighted images. USPIONs

manage to increase their blood circulation half-life to 2h resulting in an increased ability to reach the target tissue. In days duration SPIONs and USPIONs metabolized into a soluble and non-superparamagnetic type of iron and incorporated into the physiologic iron pool.[54] The EPR effect helps SPIONs to be internalized into tumors.[58] Concluding, the advantages of SPIONs as negative contrast for liver imaging and USPIONs for LN imaging have been widely reported in conjunction with their usage in angiography as a bone marrow contrast or perfusion agent within the brain and kidney because of their ability to be readily distributed in the intravascular space.[59]

DYSPROSIUM

Dysprosium possesses high magnetic moment (the largest lanthanides) and short (∼10−13 s) electronic relaxation making it a great T2 contrast agent. MSNs incorporate Dy- DOTA chelates in the outer pore channel as a modifying strategy to produce high r2 values. Gonza´lez-Mancebo et al. designed a promising contrast agent DyF3 rhombus-shaped nanoparticles with an average 110 × 50 nm size and an r2 of 380.4 mM−1·s−1 in a 9.4 T.[60] Kattel et al displays a promising T2 contrast agent d-glucuronic acid-coated ultrasmall Dy2O3 nanoparticles and Dy(OH)3 nanorods with a mean size of 20 × 300 nm. The latter showed decreased r2 value in comparison but both demonstrated optimal r2 values for potential use as a T2 contrast agent.[61] Lastly, another promising agent with high r2 values in a magnetic field of 9.4 T is β-NaDyF4.[68]

PARAMAGNETIC DYSPROSIUM DENDRIMERS

Dy(III) (G = 5) dendrimers were studied extensively as T2 contrast agents due to their relaxation properties at various magnetic fields.[63,64] The Dy-dendrimer and Dy-DOTA and Dy-DTPA single chelates expressed a 1/T2 value that increased quadratically with higher field strengths and was temperature dependent. Consequently, studies showed that utilizing this relaxation mechanism brought to fruition high-relaxivity selective T2 contrast agents (i.e., high R2/R1 ratios) that can be further enhanced by employing nonionic structural chelates like bis(methyl)amide(BMA)-DTPA complexes which are known for long τm values (Fig 12).[63,64] Nowadays an interest has been shown in the dendrimerization of

Dy(III) chelates by manipulation of the water exchange rate to manufacture high relaxivity T2 CAs.[63]

Fig 12. Variable field relaxometry of a Dy-DOTA-conjugated G = 5 PAMAM dendrimer and single Dy(III) chelates. Shown are the T2 relaxivities of (a) Dy-DOTA-PAMAM G = 5 dendrimers, (b) Dy-DOTA single chelates, and (c) Dy-DTPA single chelates as a function of magnetic field strength. [73]

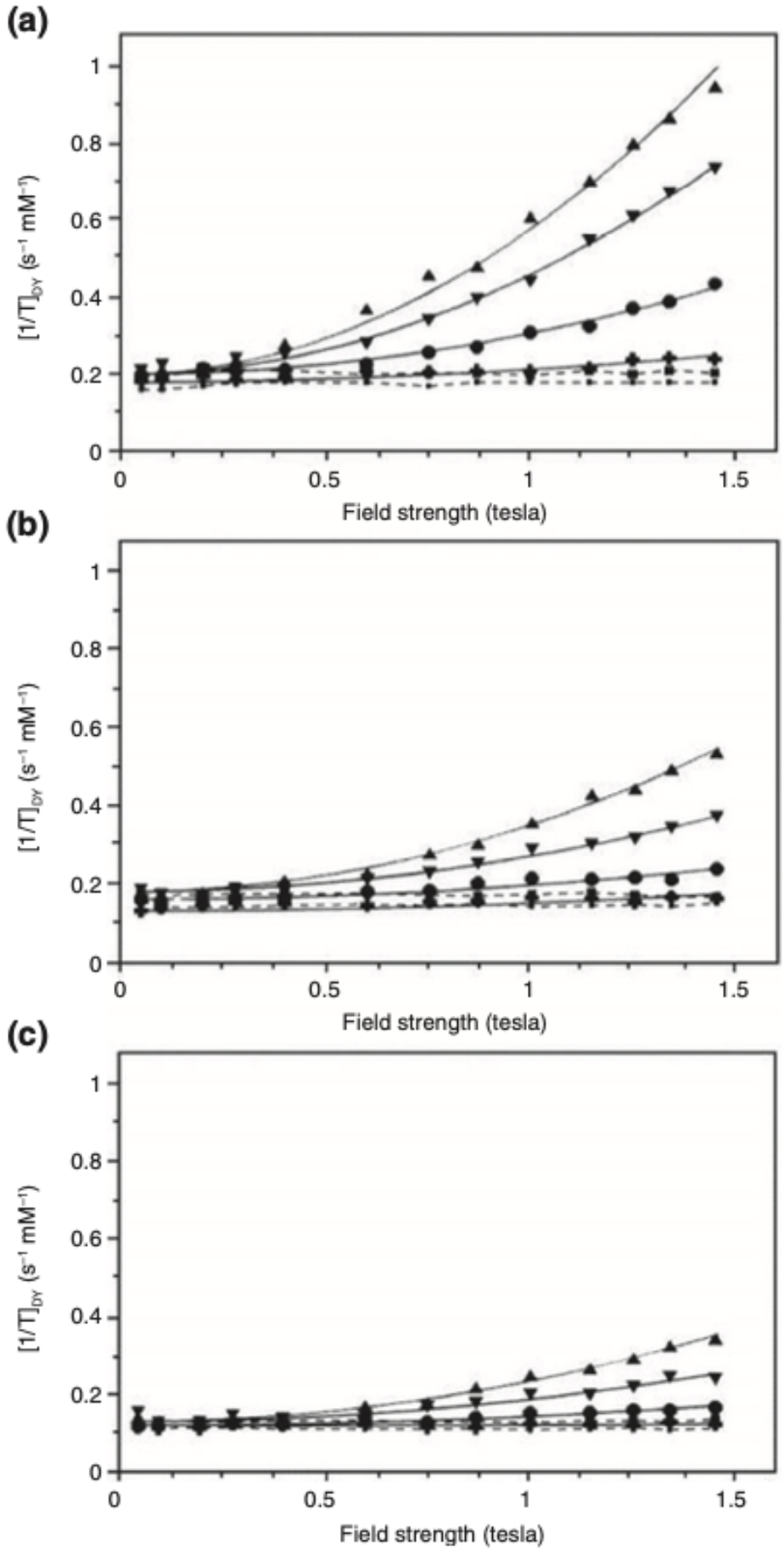
(a)
(b)
(c)
$[1/T]_{DY}$ (s^{-1} mM^{-1})
0
0.2
0.4
0.6
0.8
1
0
0.5
1
1.5
Field strength (tesla)

HOLMIUM

Table 5.
NP-based paramagnetic
Contrast agents
for MRI [74]

Material	Size(nm)	R2(nM^{-1} $.s^{-1}$)	Magnetic field (T)
NaHoF4	28.9	222.6	7
PEG-Ho_2O_3	80-90	23.5	1.5
HoF_3	94.3	608.4	9.4

Ni et al. designed a Ho3+-doped NaYbF4 with surface phospholipid-PEGylation compound for T2-weighted MRI, combining the main features of holmium which is small electronic relaxation time and great efficient magnetic moment with the Yb3+ as a sensitizer to produce high r2 and ultimately an efficient dual-modal contrast agent.[75] NaHoF4 NPs and holmium oxide NPs (Table 5) possess great potential as T2-weighted MRI CAs.[61,69]

D1.3 CEST (Chemical Exchange Saturation Transfer)

CEST has been introduced as a new way to obtain MRI scans. The technology relies on detecting exchangeable protons, such as amines or amides, present in many endogenous molecules which allows the generation of a multicolor MRI that can detect many different metabolites simultaneously. Subsequently, the detection of many metabolites, even at relatively low concentrations using endogenous, non-toxic substances holds the potential for great clinical applications. Nowadays, CEST contrast agents have been gaining traction due to their ability to be turned on and off by RF radiation resulting in MRI that can explore biochemical microenvironments in a range of different conditions such as pH, redox processes, metal ion, and enzyme concentrations. Activatable MRI CAs possess the ability to respond to a specific stimulus and precisely eliminate background signals by enhancing the ones at target sites. CEST refers to a chemical exchange between solute and solvent and provides high sensitivity through which it is possible to visualize a low concentration of solutes through water signals. The method is based on the selective saturation of exchangeable protons of endogenous or exogenous molecules while employing a specific

radio frequency (RF) pulse. The range and sensitivity of CEST contrast agents can be enhanced exponentially by the means of PARACEST. Encapsulation of the PARACEST into the NPs or agents with polymeric structures demonstrated large water exchange sites. "Smart" agents can modify their CEST response to follow changes in pH, ligand binding shift, etc. A good CEST agent is characterized by an increased chemical shift difference between both pools of protons and a slow exchange rate between the exchangeable protons and the bulk water. LipoCEST slows down the exchange rate by being incorporated into a liposome.[70] To test the effectiveness of this strategy clinical trials have begun which enlisted patients with breast cancer to investigate if the pH sensitivity of CEST can be used to detect acidosis and hypoxia in breast cancer. Furthermore, GlucoCEST is investigated as an alternative to 18F-FDG in tumor detection. Peng et al. designed a new imaging probe with fluorinated chelators which possessed symmetrical fluorine atoms as 19F ion-CEST. The 19F CEST imaging probe was able to detect with high sensitivity and specificity metal ions and saw that whenever metal ions are chelated by DTPA derivatives or EDTA derivatives lead to the modification of the fluorine electron environment and induced a 19F NMR response, chemical shift changes demonstrated and a new peak can then be observed on the 19F NMR spectra of chelators which then is saturated to demonstrate the saturation transfer to the free chelators.[71] Micelle formulation constitutes an alternative in manufacturing CEST probes in which paramagnetic complexes are copulated to micelle-forming cationic polymers through ion-pair attractions. Research groups investigated the practicality of applying polymer-based CEST probes with the ability to form micelles and reversibly dissociated into unimers in diverse pH environments gaining the ability to fip the CEST contrast from on to off and vice versa. They used tertiary amine-based block copolymers in acidic conditions resulting in the micelles dissociation into protonated unimers, turning on the CEST signal.[44] Leading them to establish the great potential of a pH-activable micelle platform as a CEST CA. Kun Na and co-workers designed a smart polymeric micelle with changeable r1 relaxivity and cancer-recognizable MRI CAs (CR-CAs) with the utilization of pH-responsive polymeric micelles.[76(p)] Gadolinium neutron capture therapy in an attempt to achieve the MRI-guided neutron capture therapy of tumor has been closely investigated by Kazunori Kataoka and co-workers with the usage of Gd-DTPA/Ca Phybrid nanoparticle.[15] The aforementioned compound displayed increased accumulation in tumors which resulted in a selective contrast enhancement of tumor

tissues and gave them the ability to precisely detect the tumor by the means of MRI. Moreover, 50% of the cancer cells were killed through neutron capture therapy and the hybrid NPs weren't toxic to the surrounding tissues giving rise to potential safe cancer treatment.[76]

D2. Recent Developments

D2.1 Paramagnetic/Superparamagnetic liposomes

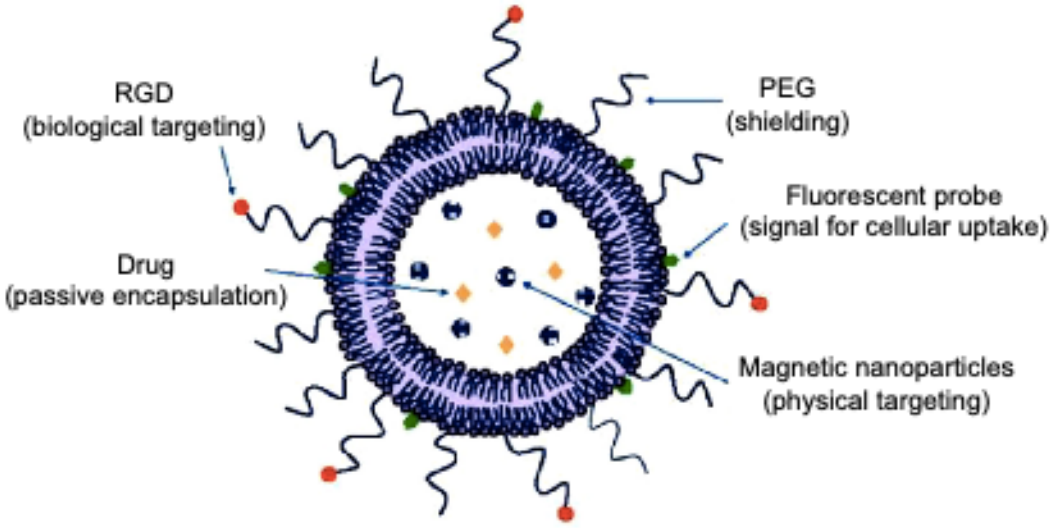

Figure 5 Scheme of multifunctional liposome for molecular imaging, drug delivery, and therapy.
Abbreviations: RGD, arginine-glycine-aspartic acid; PEG, poly(ethyelene) glycol.

[68]Fig.

The vast scope of advantageous characteristics of liposomes has made them a prime target for MRI probe manufacturing.[77] Firstly, hydrophilic substances can be encapsulated in their aqueous inner core and hydrophobic compounds in the bilayer. Secondly, liposomes because of their bio-compatibility can be used as carriers for theragnostic procedures. For example, the development of Gd-based contrast agents (paramagnetic liposomes) or iron-based contrast agents (superparamagnetic liposomes) for the aforementioned purpose has been gaining traction. To achieve this goal cell-labeling or active targeting contrast agents should be utilized to enhance the sensitivity of MRI and to develop probes that can detect

specific molecular markers of a given pathological process resulting in more personalized medical care. Colloidal structures and liposomes are usually utilized as a single carrier with multiple ligands to attach to molecular markers. Gd–DTPA and Gd–DTPA–cholesterol is encapsulated by liposomes reentering T1 MRI active.[3] Concerning sensitivity issues, a high payload of Gd-containing amphiphilic lipid can be incorporated into the bilayer which will increase the relaxivity and consequently the sensitivity.[67] The lipid composition of liposomes affects the relaxivity produced by the CAs encapsulated or incorporated within them and water diffusion at the interface with the phospholipid surface is strongly influenced by the excluded volume provided by the active lipid molecules and head groups. Consequently, the liposome's physical state and its cholesterol content can modify the contrast agents' overall impact on local tissue water relaxivity. In recent years to counteract the aforementioned issue superparamagnetic liposomes or magnetoliposomes (MLPs) have been developed and established as the primary multifunctional hybrid liposome/nanoparticle assembly. When the superparamagnetic particles were USPIONs, the MLPs would produce a T2 contrast and when the superparamagnetic particles were SPIONs, the MLPs would be used as T1 contrast agents. Initially, MLPs consisted of iron oxide cores, upon which one phospholipid bilayer was adsorbed in a size of ~20nm. Eventually, the design of an extruded MLP was introduced which comprises giant unilamellar vesicles and engulfed several small nanometer-sized waters-dispersible iron oxide cores within the aqueous cavity. With this method, the encapsulation of magnetic particles can even be achieved by sonication or inverse phase evaporation.[59] The flexibility of MPLs and lipid conjugation allows for the development of nanosystem nanosystems theragnostic potential and can be detected by a multitude of imaging methods through their ability to combine magnetic cores with drugs, fluorescent–lipid conjugates, and ligands.

MRI can detect the distribution and progress of MLPs through the body due to MLPs' active targeting either through biological targeting or magnetic targeting techniques. Leading to a minimum number of NPs needed to achieve T1 and T2 enhancement.[59] Gd ions were anchored to the surface of MLPs, with up to 500 Gd ions per magnetic vesicle. Fig[59]

D2.2. CORE PROPERTY IMPROVEMENT AND SURFACE MODIFICATION

The development of NP-based MRI contrast agents with biocompatible surfaces and more robust contrast capabilities has been the main focus of recent studies. The chemical composition and thickness of the outer surface coating of NPs have a determent factor in their biodistribution. Regarding the capacity of MRI CAs of NPs determent factor plays their core size and material. Lastly, interactions between water molecules and surface material factor into the equation.

Improvement of Core Property

Multiple studies have shown that with the increase of NP size, T2 relaxivity increases, and magnetism can be influenced by the intrinsic properties of the materials.[78]

Improvement on Shell Property and Surface Modification

Signal enhancement can be achieved through appropriate surface coating. SPIONs and USPIONs synthesized by conventional coprecipitation strategies yield NPs with polydisperse sizes and lead to a weak MRI contrast effect. So, a new strategy came into effect called thermal decomposition, and through this magnetic NPs with uniform size and high crystallinity were designed. Nevertheless, their biomedical applications in aqueous media are dampened due to their hydrophobic surface. Consequently, surface modification has been deemed a necessity to add function capabilities to magnetic NPs. Nowadays, a variety of surface modification strategies exist such as shell formation, ligand exchange, and micellar encapsulation.[79,80,81] The oleic acid ligands on NPs through a ligand exchange process are being replaced by bifunctional hydrophilic ligands and the ligand exchange process follows either a stripping or biphasic protocol.[82] The biphasic protocol is a one-step process that is based on the competition between two ligands. On the other hand, the stripping process is a two-step process that requires removing the oleic acid on the nanoparticle surface and adding new hydrophilic ligands. Consequently, the phosphonic acid and carboxylic acid decreased saturation magnetization and relaxivity, but catechol-type anchors such as dopamide-PEG and 2.3-dihydroxy-benzamide-PEG resulted in magnetic properties comparable to control molecules. Furthermore, the biphasic method yielded NPs of smaller size. Nonetheless, MIONs that underwent ligand exchange via the biphasic protocol expressed higher relaxivities than NPs produced by the stripping protocol; and higher monodispersity than the stripping method. Another strategy to

modify the NP's surface is inorganic shell formation which enables surface functionalization and shields magnetic nanoparticles from undesired oxidation of reactive species. Pierre and coworkers designed iron oxide gold nanocomposites as MRI Cas with augmented saturation magnetization. The Fe_3O_4 core underwent ligand exchange with either catecholate or PO_4 anchoring groups subsequently the surface was coated with Au NP making them attractive candidates for multimodal cell imaging. Silica-coated SPIONs are prepared via a reverse-micelle sol-gel technique and display increased T2 relaxivity. Subsequently, PEG was utilized to improve colloidal stability.[84] Moon and Hyeon designed a drug carrier that displayed the multitude of diverse capabilities of magnetite NPs coated with a mesoporous silica shell, where the silica was doped with a fluorophore. Lastly, through micelle encapsulation hydrophobic NPs can achieve enhanced colloidal stability, additionally vesicles assembled from block copolymers show potential as a nanocarrier for hydrophobic anticancer drugs, such as paclitaxel, camptothecin, and DOX.

D3. Activatable or Smart nanoprobes

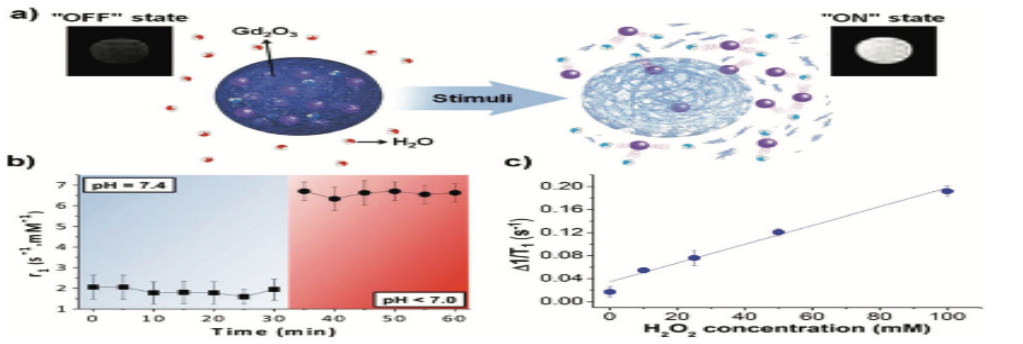

Fig. 19 (a) Schematic of how a degradable polymer matrix is able to control the interaction of water molecules with Gd_2O_3 NPs (purple spheres). (b) Magnetic relaxivity of Gd_2O_3 NPs encapsulated in pH-responsive materials demonstrates a jump from neutral pH to mild acidity. (c) Increasing concentrations of H_2O_2 results in corresponding increases in the T_1 relaxation rates of Gd_2O_3 NPs encapsulated in an H_2O_2-responsive polymer. Reproduced with permission from ref. 131. Copyright 2013, American Chemical Society.

''Activatable'' or ''smart'' nanoprobes can be utilized as high relaxivity CAs due to their easily modifiable self-assembly /disassembly relaxivities and provide highly sensitive MRI in a variety of pathological processes. A self-assembly strategy requires a trigger which can be either enzyme, receptors, redox status, or molecular interactions so NPs can stay in

circulation for an extended amount of time and the tumor can be transformed into an outsized structure leading to better MRI images.[85,86,87] The disassembly strategy offer manipulation of the tumor microenvironments to release CAs confined in NPs resulting as well in an enhanced MRI signal. Liang and associates developed the self-assembly of Gd3+-based NPs combining 1,2-aminothiol and 2-cyanobenzo- thiazole.[88] Subsequently the smart nanoprobe was activated through disulfide reduction and generated 1,2-aminothiol groups to react with the cyano groups on 2-cyanobenzothiazole leading to the self-assembly of huge Gd3+ NPs with increased relaxivity. Ye et al. followed the path of redox-activatable self-assembly to develop a probe with caspase-3/7 (an early marker of apoptosis) activated Gd-based CAs which could self-assemble into Gd3+ NPs upon reduction and activation by the marker. Highlighting the potential of in vivo enzyme activity MRI by establishing the high r1 and increased retention time that the self-assembling CAs had in apoptotic tumors. Ai et al. demonstrated the increased magnetic properties and higher r2 values acquire red from the self-assembly of small magnetic NPs into nanoclusters to extend the adequate magnetic size. In the study was reported the clustering of monodispersed iron oxide NPs inside the core of polymeric micelles. In comparison to single-core nanoparticles, multi-core nanoclusters, self-assembled from 13 nm iron oxide NPs had higher Ms values and consequently greater contrast enhancement and better MRI performance. Mao and associates stated that ultrafine iron oxide NPs with increased T1 relaxivities exhibited prolonged circulation time and self-assembled thereby switching from bright T1 contrast to dark T2 contrast in MRI. Gao and associates created Fe3O4 NPs which were modified with a responsive peptide sequence, which enabled GSH-triggered self-assembly of Fe3O4 NPs within the tumor microenvironment and also the shaping of aggregates via inter-particle cross-linking reactions. Subsequent experiments showed that such a self-assembly strategy provided a greater MRI performance. Generally, disassembly strategies possess the ability to turn the relaxivity of CAs from ‘‘off’’ to ‘‘on’’ after responding to pathophysiological parameters like low pH value and high GSH concentration within the tumor leading to an enhancement of the signal in the area of interest and eliminating the signal from background tissues to increase the specificity and sensitivity of contrast agents.[89] The r1 of the ultra-small Gd2O3 NPs under a disassembling strategy in the presence of H2O2 and under acidic conditions which are characteristic conditions of many tumors (Fig. 19a). The encapsulation of ultra-small Gd2O3 NPs within pH-responsive

polymer particles led to the deactivation of their contrast enhancement at pH 7.4. Nevertheless, burst degradation was reported at pH 6.5 which led to fourth fold enhancement of r1 (Fig. 19b). The utilization of a peroxide-degradable polymer to encapsulate ultra-small Gd2O3 NPs further confirmed a general disassembly strategy (Fig. 19c). In conclusion, pH-responsive MRI came into fruition by discharging Mn2+ from the disassembled matrix at low-pH sites which yielded high relaxivity CAs. [89]

D4. Nanotechnology for Image-guided Surgery

The overall management of cancer requires a multidisciplinary approach to achieve early diagnosis, and adequate treatment and ultimately increase the overall survival rate. Surgery is the mainstay of treatment when the cancer is diagnosed at an early stage. A key goal of cancer surgery is to attain R0 resection, which indicates a microscopically margin-negative resection. The development of targeted optically-driven visualization tools and sensors to guide minimally invasive procedures with cellular-level precision, enhance surgical vision, and supply real-time structural-functional imaging assessments signifies the future of surgery. Real-time image-guided surgery can come to fruition by utilizing optical imaging techniques such as Raman, PAI, and fluorescence.[90,91,92,93] Cancer theragnostics are gaining traction in precision surgery navigation with the development of multifunctional nanoplatforms that integrate optical and medical imaging technologies. Nowadays, leaps toward the real-time intraoperative identification of residual disease have been made by the use of targeted near-infrared fluorescent (NIRF) and surface-enhanced Raman scattering imaging probes to judge surgical margins. NIRF-image-guided surgery which uses 5-aminolevulinic acid (5-ALA) provides great tumor visualization in patients with malignant glioma enabling complete oncological resection and increased overall survival rate. The clinical translation of assorted Raman NPs is the main focus of many ongoing research and will be used by NIRF imaging for solid tumors like lung cancer to better visualize tumor margins and lead to complete resections. Kircher et al. published the use of Raman NPs in glioblastoma-bearing mice which led to their accumulation into the tumor for days and a triple-modality MRI-based photoacoustic imaging-guided intraoperative resection was achieved with negative tumor margins.[94] Regarding thoracic surgery the use

of ultra-sensitive Raman imaging has the potential to detect and delineate through the combination of high-resolution tissue-penetrating photoacoustic imaging and tumor-homing Raman NPs deep unreachable by palpation parenchymal tumors. Consequently, highlights the enormous potential of translating emerging nanotechnology platforms to thoracic surgery to enable precise tumor imaging and radical tumor resections in patients with lung cancer.

i. INTRAOPERATIVE

The field of image-guided surgery has seen exponential advancements regarding imaging techniques and agents that already are in clinical use or the last stages of clinical trials. The goal that needs to be achieved is intraoperative cancer diagnosis and precise tumor margin resection so image-guided surgery utilized optical imaging technologies to bring this goal to fruition. Cho et al. reported the use of poly (ethylene glycol)-block- poly(ε-caprolactone) (PEG-b-PCL) micelles as an apoptosis targeted-NIR fluorescent probe and a neoadjuvant chemotherapy (NACT) carrier for the precise detection and surgical resection of the tumor with the NACT IP administration. The two polymeric systems were administered in a 24h interval to an ES-2-luc-bearing xenograft m model with ovarian cancer which enabled the visualization of therapy-induced apoptosis during operation. Subsequently, the signal that was detected from the probe could be visualized two days after the IV administration. The report showed that the apoptosis targeting peptide, GFNFRLKAGAKIRFGS, showed increased accumulation in cancer vs the non-targeted NIR-micellar imaging probe. Concluding, the use of optical imaging intraoperative yields ~90% tumor resection compared to ~30% by the control group. Nanoplatforms-based optical imaging is making considerable progress and has the potential to bring image-guided surgery to everyday clinical operations.

ii. *Fluorescence Imaging*

The FDA approved ICG and fluorescein sodium as fluorescent probes in fluorescence-guided surgery. NIRF imaging gained an augmented interest in IGS due to NIR light's ability

for deeper tissue penetration with decreased absorbance and less scatter than visible light.[74] Rosenthal and colleagues designed tumor-specific fluorescent probes for intraoperative tumor imaging and delineating by conjugating antibodies onto fluorescent agents.[4] Additionally, OTL38 a NIRF agent binding with folate receptor-α undergoing clinical trials for patients with ovarian cancer and separately for patients with pulmonary adenocarcinoma.[95] Zhang et al. summarized the recent development in targeted fluorophores and their usage in real-time intraoperative imaging. [73] Cheng's team utilized nanoprobes to increase tissue penetration and tumor retention of NIRF imaging to ultimately guide FGS. The vesicles visualized tumor vasculature and lymphatic drainage for precise IGS and SLN mapping. [96] H1, encapsulated into (H1 NP) and injected via IV route to the mice.[97] SXH was designed by conjugating 4 COOH groups of H1 with PEG1000, and SDH was designed by the conjugation of αvβ3 and H1.[98] Both were able to visualize the U87MG tumors. Concluding, the NIR-II window fluorophore constitutes a great step for the clinical application of FGS.

iii. PAI

PAI owing to the photoacoustic effect has the potential to break the limitation of optical diffusion together with the increased scattering of photons in tissues. PAI is an attractive option for IGS and utilizes the high spatial resolution, 3D U/S images, the synergistic action of the high contrast and specificity, and deep tissue penetration. Three PAI systems have been developed PA microscopy, PA endoscopy (PAE), and PA tomography/CT. Kim et al. designed a golden carbon nanotube conjugated with anti-lymphatic endothelial receptor to be attached to a lymphatic endothelial receptor. Through the utilization of this nanotube as a PA and photothermal contrast agent the visualization and mapping of lymphatic vessels were possible with great NIR contrast. Pan and colleagues studied SLN mapping through the lens of the effect of size and payload of gold nanobeacons (GNBs). Concluding that the bigger the size and high payload resulted in poor transport efficiency. Semiconducting polymer NPs (SPNs) can detect tumors, LN, and the surrounding vasculature and guide cancer management by their development as PA contrast agents. Li and Pu studied the different types of SPN-based PA probes and demonstrated their potential as a viable option for LN biopsy or tumor resection. The PAE can be used in

endoscopy, laparoscopy, and thoracoscopy to guide biopsies and minimally invasive surgeries with complete tumor resections. To improve the temporal resolution of PAI contrast agents their optical characteristics needs to be optimized and this can happen with the development of NIR- II-absorbing PA probes or multimodal imaging probes that combine PA and other imaging modalities.[4] PAI utilizes ICG as a contrast agent to map the sentinel LNs. VEGF-targeted fluorescent bevacizumab-IRDye800CW is undergoing clinical trials for its utilization in breast cancer. Applications in ovarian and breast cancer involve the use of folate conjugated to fluorescein isothiocyanate (folate-FITC). Lastly, the combination of ligands such as matrix metalloproteinases or cathepsins, and proteases with fluorescent dyes can be used to detect tumors and these fluorescent probes are activated by enzymes of the tumor's microenvironment characteristics.

iv. Surface-Enhanced Raman Spectroscopy

Raman spectroscopy (RS) is a promising analytical procedure for disease diagnosis due to its excellent sensitivity and specificity.[99] A major drawback in the aforementioned endeavor is its weak scattering effect, to counteract this drawback electromagnetic or chemical enhancement via surface-enhanced Raman scattering (SERS) has the potential to be used in IGS.[99] Additionally, SERS-based contrast agents provide higher TBR and greater photostability than fluorophores (ICG).[100] SERS/SERRS nanoprobes constitute 3 parts: a Raman reporter layer, a metal core, and a shell (Figure 7a) which gives the nanoprobe biocompatibility, stability, and the ability to be conjugated with targeting molecules on the surface (Figure 7c) or it could be radiolabeled for multimodal imaging (Figure 7e,f). Subsequent coating provides control of the plasmon properties for a good scattering effect. [,101,102,103,104] Intraoperative SERS/SERRS finds application in tumor resection and MRD detection. Kircher's team designed a SERRS-nanostar which was administered IV and consisted of a gold core (75 nm), coated with a Raman dye (IR780 perchlorate) and silica with PEG conjugation and SERRS imaging was obtained. The experiment showed that SERRS-nanostar could visualize tumor margins and MRDs of various cancers (brain, ovarian, pancreatic, liver, and breast). Furthermore, SERRS endoscopy detected other pre-cancerous gastrointestinal lesions. Gambhir's group created a CA9- and CD47-targeted SERS NPs (s420-CA9 and s440-CD47, Figure 7c); and combined SERS imaging with a

cystoscope system (multiplexed Raman cystoscopy) in an attempt to differentiate bladder cancer (Figure 7d).[4]

The aforementioned experiment provided a great example of the application of minimally invasive surgery with the use of Raman endoscopy and laparoscopy. The goal of treating cancer at a molecular level is the cornerstone of cancer management and NIR optically-active nanomaterials and dye encapsulation within silica nanoparticles serve as modifications that can maximize tumor-to-background ratios resulting in greater detection sensitivity. A high-resolution whole-body optical imaging strategy demonstrated by a multispectral optoacoustic tomography with the ability to detect through ultrasound optical absorption and can reach depths greater than those achieved by fluorescence imaging. The aforementioned technique utilizes a range of light-absorbing nanoparticles (gold nanorods) and endogenous chromophores resulting in high-resolution optical assessments which can provide accurate measurements of deep tissue perfusion and viability. Leading to optically-active particle probes for intraoperative cancer management with molecular specificity for IGS. Nowadays, it's estimated that fluorescence-enhanced surgical vision can transform the surgical field by increasing the overall sensitivity and specificity of surgical procedures while offering detection of MRD with single-cell precision. Developing a personalized treatment plan can be assisted by acquiring intraoperative structural imaging information together with functional optical imaging evaluations which give rise to real-time treatment management based on: tissue imaging assessments with 3D maps of tissue functionalities such as oxygenation and perfusion and lastly, volumetric images of lesions for surgical navigation. Targeted particle radiotherapies and radiosensitizing NMs with high atomic number (Z) possess the ability to significantly increase the radiation dose without any damage to the surrounding tissue resulting in more efficient cancer treatment. Robotic-assisted surgery marks a promising future for the combination of endoscopy and advanced nanotechnology tools.[105] Using nanotechnology as sensors, imaging, and navigation in the robotic field can highly benefit and increase the surgeon's ability, especially in the field of cardiothoracic surgery.[106,107] In atrial fibrillation the use of a remote image-guided magnetic catheter guidance device promises great success. Robotic-assisted catheter technology is utilized in mitral valve repair, coronary artery bypass procedures, and in assisting in septum myectomy in hypertrophic obstructive cardiomyopathy.[108]

v. Poly (Allylamine) Hydrochloride

ICG is the only FDA-approved NIR dye that has been investigated for sentinel LN mapping. ICG can be encapsulated into poly (allylamine) hydrochloride chains cross-linked ionically with sodium phosphate. Bahmani et al. studied the aforementioned method and functionalized it with PEG to create a nanocarrier that can be used as a template for targeted molecular imaging of a highly specific biomarker related to ovarian cancer.[109]

Figure 7. SERS nanoprobe. a) Schematic and TEM images of their construction. b) preoperative imaging via Raman microscope on the left and IGS via hand- held Raman scanner on the right. c) Designs of the CA9-, CD47-targeted SERS NPs , passive-targeted IgG4 NPs. d) Invasive bladder cancer visualized via multiplexed Raman imaging with SERS e) PET/Raman-IGS made possible via the design of chelator-free radiolabeling PET-SERRS NPs. f) A triple-modal nanoprobe , MPR, for MRI/PA/ Raman-IGS.[4]

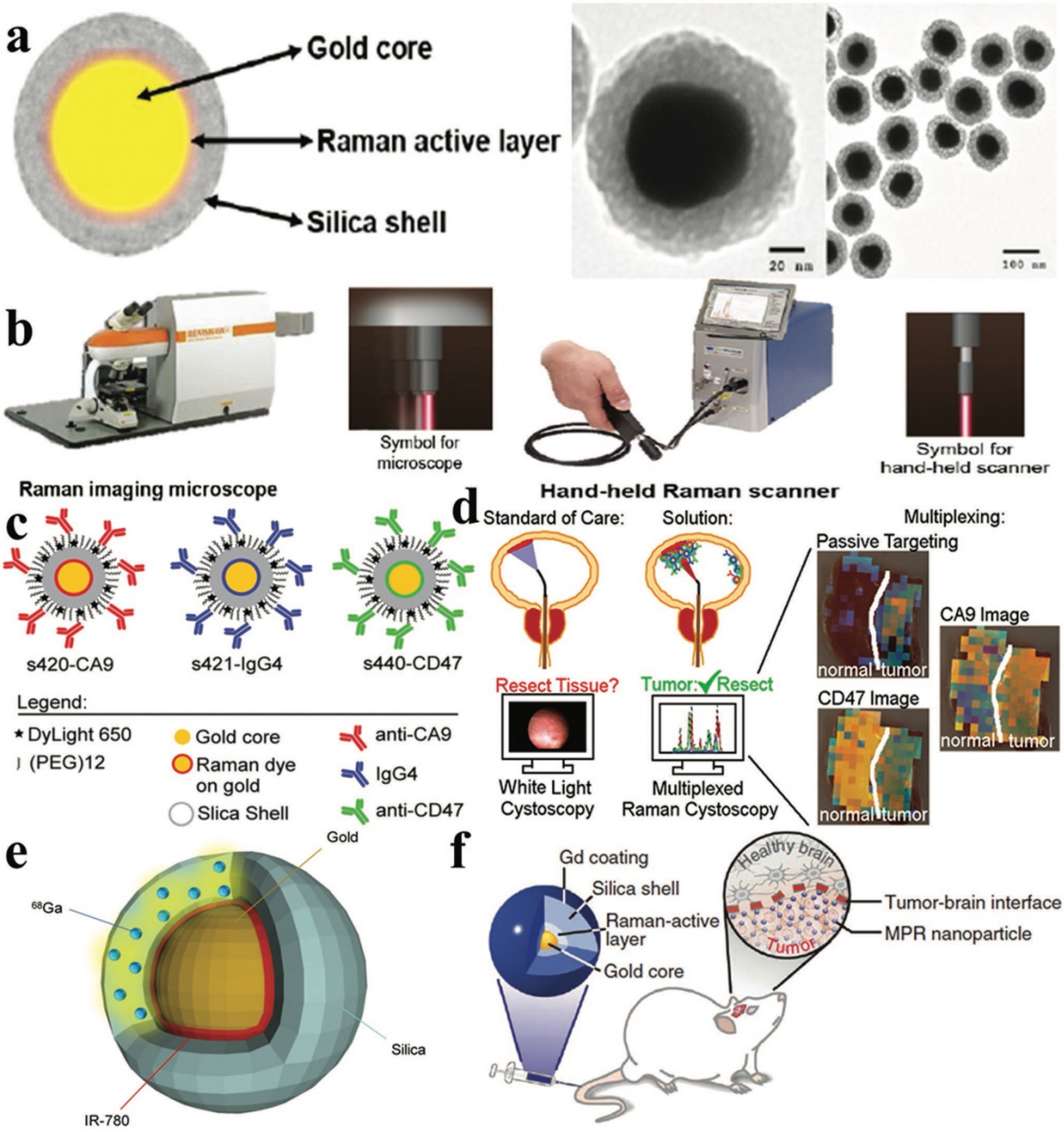

vi. Detection of Micrometastasis

Complete and total elimination of all malignant cells is the mainstay of cancer treatment. Ensure that all remnant cancer cells should be identified and removed together with the primary tumor otherwise has been estimated that a ~20-40% will experience a relapse of their disease. Recent clinical trials utilized intraoperative fluorescence imaging to detect breast cancer cells in patients. Real-time intraoperative fluorescence imaging provided

doctors with a better management plan and prevented redo surgeries for patients with positive surgical margins. MRI which is the imaging modality of choice for most cancer fails to detect micrometastases. The definition of micrometastasis is cancer tissue that doesn't exceed 0.2-2mm in length in the maximum dimension. Silica nanoparticles that coat gadolinium chelates and coupled with fluorophores QD possess the ability to achieve better tissue penetration for MRI and fluorescence imaging modalities. For instance, silica-coated PEG-ylated QD embedded in gadolinium was detected through T1-weighted MRI imaging of colon cancer cells the third day after injection before even the tumor vasculature was developed and the size of the tumor was less than 2mm in diameter. Precise real-time IGS developed through molecular imaging technologies for theragnostic applications. The sentinel lymph nodes (SLNs) constitute the primary site for various cancers that metastasize through the lymphatic route. Consequently, the biopsy of SLNs has a prognostic value. Recently, improved optical diagnostic systems utilized to detect the SLN without the need for blue dye or radioactive tracer. The characteristics of a nano theragnostics system for the aforementioned purpose should be small enough to travel through the lymphatic system and also large enough so they aggregate to the SLN and be visualized. An SLN detecting probe should possess great intraoperative photostability. A biodegradable pullulan-cholesterol polymer nanogels labeled with fluorescent IRDye800 was created by Noh et al. for this purpose. The labeled-NIR dye probe was administered intradermally into the mouse and 30 min after injection the nanoprobe was aggregated into the SLN and was able to be detected. Koyama et al. designed a dual-labeled imaging nanosystem with a dendrimer-based contrast agent. Preoperatively the MR detected the tumor's location and the Cy5.5 fluorescent signal guided the real-time intraoperative SLN detection and provided highly precise data. The significance of the dual imaging agent presented in the preoperative detection of the SLN location by MRI and in the increased sensitivity of the fluorescent signal which was able to visualize axillary LN that wasn't detected in the MRI. Subsequently, the dual-probe detected micrometastasis in healthy mice and orthotopic head and neck tumor-bearing mice. IGS with the use of optical images has met many drawbacks such as the small amount of obtainable targeted near-infrared (NIR) agents, rapid photobleaching, superficial tissue penetration, an inability to detect multiple cancer, and limited contrast resolution. To counteract these drawbacks a variety of optically-active and targeted imaging agents, including particle-based probes have been

developed. These probes offer real-time early-stage molecular detection and treatment of disease with clinical-grade accuracy. Additionally, these probes possess the ability to identify tissue-specific biomarkers which will result in reliable staging, and accurate identification of cancerous nodes, margins, and adjacent innervation together with precision-based treatment. The integration of high-resolution intraoperative camera systems which enables the detection of lesions smaller than 60 µm and robotic-assisted surgical equipment represents a significant clinical advance and the future of surgical oncology. Nowadays, direct neoplastic cell detection is the focus of manufacturing new endogenous tissue contrast or non-specific optical agents, like indocyanine green (ICG). To achieve the aforementioned goal and labeling specificity various targeted and optically-active imaging products, such as antibody-peptide-dye conjugates and targeted molecular probes were designed and await clinical application.

vii. *Multimodal Intraoperative Imaging*

In theory, complementary and exponential strength can be achieved through the combination of multiple imaging modalities. Alves et al. designed a multimodal contrast agent (cRGD-800CW-TCO) through conjugation of a cyclic arginine–glycine–aspartic acid (cRGD) peptide with a NIR fluorophore (IRDye800CW) and a trans-cyclooctene (TCO) tag. cRGD-800CW-TCO which combined the fluorescence and PAI methods to achieve deep tissue penetration, high spatial resolution, and overall increased specificity. On the other hand, Chen's group introduced a ferritin-loaded (DFRT) nanocage for PA/fluorescence multimodal imaging probe which demonstrated increased photothermal conversion efficiency for PTT. Wang and associates designed a Cypate-grafted gadolinium oxide nanocrystal (Cy-GdNC) for NIRF/PA/ MRI with the utilization of biomineralization. Tian's group demonstrated a NIRF/PA nanoprobe (ICG-loaded Au@SiO2) which demonstrated great tumor detection. Although the aforementioned groups used multimodal imaging to guide PTT or detect tumors, the application of these NMs in IGS and synergetic cancer management can’t be overshadowed.

Jokerst and colleagues designed a gold nanorod (GNR) that combined PAI and SERS modalities for image-guided surgery in ovarian cancer. PAI detected the tumors and SERS

provided the IGS. MRI is the gold standard in neurosurgery to identify brain tumors and via CAS systems guide stereotactic surgery. Kircher's group displayed a bimodal nanoprobe (Cy5.5-CLIO) which was designed by a NIR fluorophore (Cy5.5) to provide intraoperative fluorescence imaging and an iron oxide core to be utilized in MRI for tumor detection. Subsequently, they designed a multimodal MRI-PA-Raman probe (MPR NP) which features the structure of SERS NPs with Gd3+ iron coating. The probe could visualize the glioblastoma with MPR NPs accumulating and displaying the tumor margins plus micrometastasis depicted through Raman imaging.[4]

Yue and associates displayed an EGFRvIII-targeted MRI/SERRS nanoprobe (AuP-FAL) which guided the resection of EGFRvIII+ glioblastoma by a handheld Raman scanner. Moreover, a variety of MRI-based multimodal imaging probes has been introduced for IGS, including Gd-Ag2S nanoprobe for MRI/NIR-II fluorescence imaging, ICG-coated SPION clusters (ISCs) for MRI/PAI, and endoglin-targeted nanoprobe Den-Apt1 for MRI/ NIRF imaging.[4]

Porphyrins constitute promising agents for imaging and disease management due to their innate photophysical and photochemical properties. Porphyrin-based molecules are utilized in theragnostics for PT, MRI, and fluorescence-guided surgery. AIEgens have emerged in the last 20 years as great luminescent materials because of their unique characteristic to be non-emissive in dilute solution but become highly emissive through the restriction of intramolecular motion in an aggregated state. AIEgens possess excellent biocompatibility, increased sensitivity, and great fluorescence properties. Consequently, AIE NPs are investigated as an innovative theragnostic tool for gene therapy, fluorescence imaging, PDT, and chemo in cancer management. Liu et al. designed a NIR fluorescent-DTPEBBTD-C4 NPs and NIR emission for IGS in tumor resection. this resulted in accurate tumor detection and resection even for tumors less than 500 mm in diameter.

viii. NEUROSURGERY

A neurosurgical probe of OCT offers an intuitive view of the brain parenchyma and together with its endoscopic, needle-type, hand-held and various robotic arms probe can provide excellent detection of tumor margins.[77] Böhringer et al. designed a rigid endoscopic probe to mount an OCT device to achieve intraoperative real-time detection and resection of

brain tumors.[3] Liang et al. and Sun et al. took into consideration the need for easier-handled equipment in the operation room and designed a needle-type forward-imaging OCT probe that could utilize minimally invasive equipment. Zhang et al. utilized the dual (GPU) graphic processing unit to accelerate the FD-OCT system and reentered it valuable as intraoperative microscopic guidance.[67] Real-time intraoperative identification and histological diagnosis of brain tumors is a linchpin for neurosurgery. Figure 5 demonstrates how OCT attenuation maps helped the neurosurgeon before and after surgery to identify and distinguish cancerous from healthy tissue. The multimodal imaging system offers tumor resection under neurosurgical guidance. Liang et al. explored the combination of OCT with an MRI-compatible needle-type probe to provide real-time in situ imaging of tumor architecture and resection under neurosurgical guidance. In an attempt to aid surgeons by providing them with a magnified view of the region of interest, intraoperative real-time tumor margins, and precise tumor structure an integrated system of photoacoustic OCT and the surgical microscope was introduced. The main drawback of the aforementioned endeavor is that could lead to a large-scale/wide-field scanning of the zone of interest where scanning the perpendicular surface and translating it to an intraoperative visualization of 3D data. The combination of OCT imaging with a binocular microscope can provide the precise depth information and detect micrometastasis. Robotized operating microscope-integrated OCT imaging can scan a larger surface and provide higher resolution and an intuitive viewing so precise surgical tumor resections can be performed. Real-time treatment of malignant tissue can be performed through integrated OCT and a laser ablation system. OCT-guided laser ablation constitutes a new theragnostic technique for brain tumor resection and management. OCT can monitor and capture the dynamic changes in the tumor microenvironment during laser ablation. Nowadays, OCT-guided laser surgery is utilized in ophthalmic surgery. Meng-Tsan Tsai et al. introduced an OCT-guided laser-assisted drug delivery system to monitor drug diffusion by the means of induced microthermal ablation zones. Lastly, in the nearby future, the mixture of data from morphological and functional imaging of brain tumors will increase the demand for clinical applications for OCT in neurosurgery. Together with the development of a new optical attenuation coefficient and artifact intelligence-based approach to OCT image processing will enable the real-time identification, classification, and segmentation of malignant tissue and a more personalized approach to neurosurgery will unfold.[78]

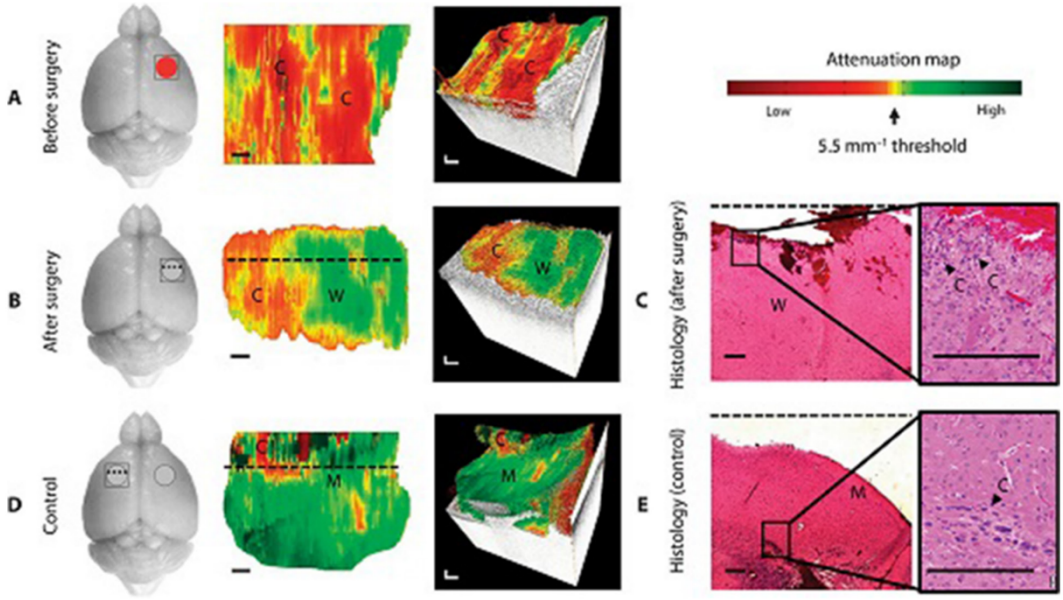

Figure 5. *In vivo* OCT imaging brain cancer in a mouse with patient-derived high-grade brain cancer (GBM272). [110]

ix. Mapping Sentinel Lymph Nodes (SLNs) for Surgery

Currently, in clinical application, LN mapping methods include blue dyes, fluorescence imaging, and radionuclide. Furthermore, the use of injectable carbon NP suspension for the aforementioned goal is widely known. The gold standard for sentinel LN detection is the combination of a dye and a radionuclide. Radionuclide-labeled nanomaterials as LN tracers are highly sensitive but suffer from their inability to distinguish SLNs from other DLNs.[4]

To counteract the aforementioned challenge indium-based QD was introduced. Recently studies that compare the effectiveness of cadmium/tellurium QD to methylene blue have been taking place with the results showing the superiority of the QD. QD experienced a faster onset of action and its fluorescence signal was detected 24h post-injection compared to 2 h of methylene blue. Additionally, QD conjugation utilizing its electrostatic attractions to hyaluronic acid, and anionic glycosaminoglycan abundant in the matrix of the connective tissue resulted in LN visualization. The astonishing phototunable features of QD have been

used for multicolor applications. Multiple recent QD studies demonstrated deep tissue penetration and easier detection of SLN through photodynamic fluorescence imaging with self-illuminating CdTe/CdS QD, also known as QD-bioluminanceance resonance energy transfer (BRET) conjugates. Nano-contrast agents have been thoroughly investigated for LN detection due to their favorable biochemical characteristics.[80] A major feature of a potential LN tracer should be the balance between diffusion and retention rates as well as optimal administration for IGS. Superparamagnetic iron oxide nanoparticles (SPIONs) possess the ability of a radioisotope-free technique for SLN detection which has demonstrated equal sensitivity to the gold standard. Moreover, the benefits of SPION for LN detection include their route of administration, which can be given intravenously and interstitially, which provides the surgeons with an effortless hand-held probe that can guide intraoperative resection and histopathologic evaluation of SLN as well as facilitate preoperative biopsy with MRI. Resulting in a precise and cost-effective diagnosis of LN metastasis that can become a clinical norm in the near future. NIR-II imaging navigation gained traction because of its stronger lymphatic fluorescence with a lower quantum yield (QY) but higher signal-to-background ratio (SBR), which was superior to ICG. Antaris and colleagues describe the aforementioned method with a NIR-II fluorophore (CH1055-PEG) which achieved the aforementioned goal and also was excreted through the kidneys in 24h. CH1055-PEG provided an image that could last for 5-7h postinjection making it a promising application for intraoperative LN mapping and IGS. Cheng et al. designed a diketopyrro-lopyrrole-based semiconducting polymer NP (PDFT1032) which experienced a high tumor-to-background ratio (TBR) and utilized it for IGS and SLN mapping (Figure 1a). Intradermal administration of PDFT1032 took place and SLN was detected and resected to verify metastasis via histopathology analysis (Figure 1b). Furthermore, complete tumor resection was achieved through intravenous administration of PDFT1032 via NIR-II imaging in a mouse with osteosarcoma, subsequently, micrometastasis and LNs were identified as well (Figure 1c). Furthermore, PAI can offer high soft-tissue contrast that is of utmost importance in LN mapping. Organic semiconducting NMs offer great biocompatibility and biodegradability is investigated in PAI. Pu et al. displayed how the lymphatic system can be visualized by the PA signal even 24h after injection of a semiconducting NPs (SNPs), later autopsy showed the accumulation of SNPs in the LNs, thus making it another viable option for LN mapping. Chen's group investigated LN mapping via the prism of dual-modal imaging

of positron emission tomography (PET) and PA (Figure 1f,g) as well as the size-dependent effect of semiconducting perylene diimide (PDI) NPs (Figure 1d,e). In the study, various PDI NPs were created and labeled with radionuclide 64Cu for PET. Chen's group concluded that the 100 nm NPs offer the optimum LN mapping results. A 1h window for SLN biopsy was given and followed by a rapid histopathologic estimation to facilitate an intraoperative surgical decision (Figure 1h). Memorial Sloan Kettering Cancer Center recruits for a clinical trial on targeted silica NPs for real-time imaging-guided intraoperative mapping of LN metastasis (ClinicalTrials.gov) Identifier: NCT02106598). In this trial, cRGDY-PEG-Cy5.5-C dots map SLN in melanoma patients through a hand-held camera system. [4]

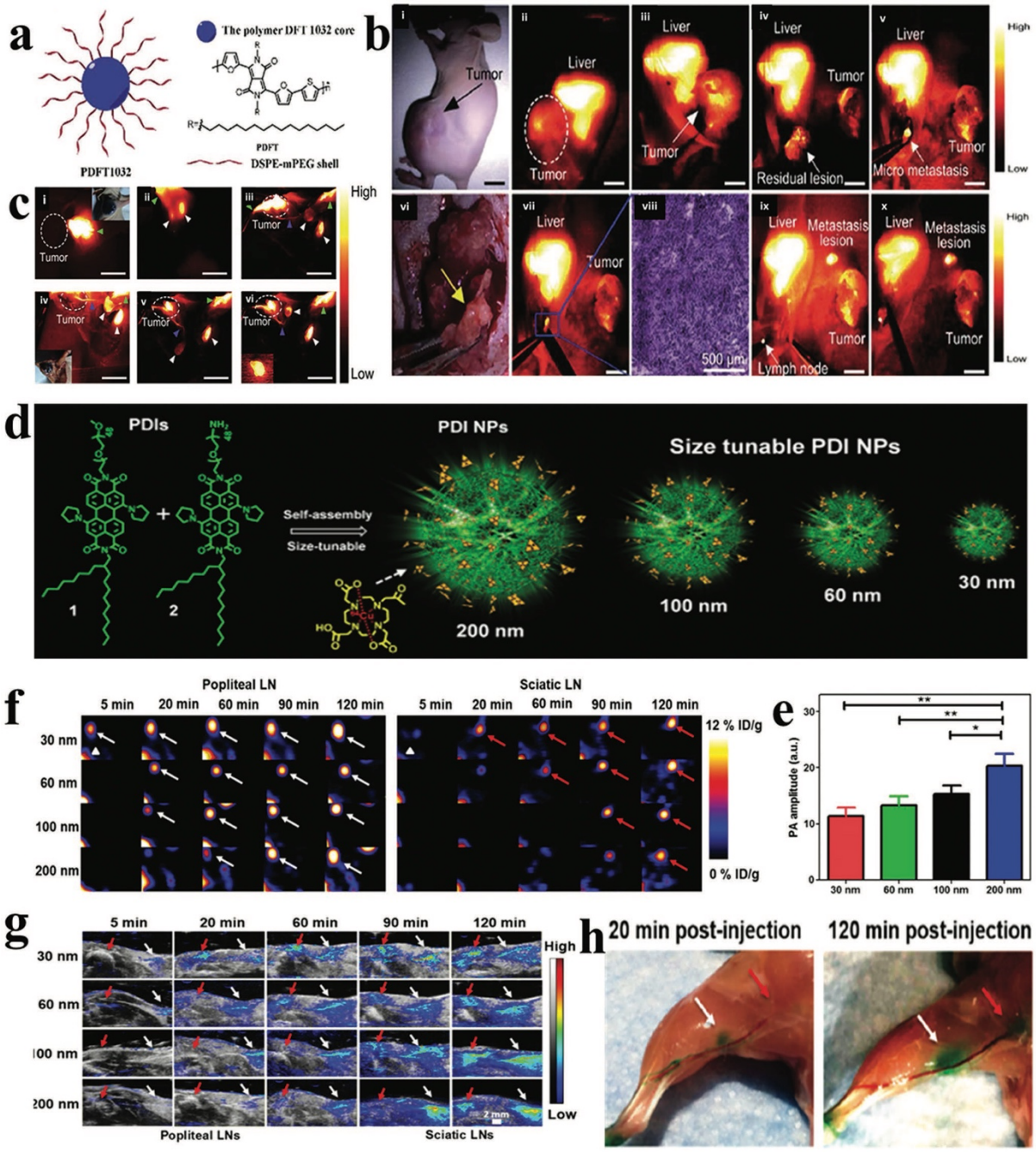

Figure 1. An image guided SLN mapping and tumor resection via the construction of PDFT1032 and size-tunable PDI NPs. a) The PDFT1032 NP. b) A mouse with melanoma underwent biopsy via NIR-II imaging-guided for SLN mapping. i–v) The digital images, PDFT1032 (white dashed circle: the B16F10 melanoma, green arrowhead: the PDFT1032 injection site). vi–x) After SLN resection with pathohistological positive results c) (white dashed circle: osteosarcoma, white arrow: the residual lesion) in NIR-II IGS. d) Size-tunable PDI NP the formulation. e) PA amplitudes of different-sized PDI NPs at 680 nm at the same optical density. f) PET images, and g) ultrasound images of size-dependent uptake in popliteal LNs and sciatic LNs at different time points post-injection. h) LN mapping with PDI NPs at 20- and 120-min post injection, all white arrows (d)–(h) represent popliteal LNs, red arrows represent sciatic LNs. [111]

D5. Theragnostics

Choi et al. designed the hyaluronic acid (HA)-based self-assembled NPs for tumor targeting with the usage of both active and passive targeting. They used PEG as coating and reported a reduced off-target effect within the liver and prolonged blood circulation. Additionally, they noticed that HA conjugated with a peptide molecule displayed great advantages in clinical imaging due to dual responsive (redox and pH stimuli) making it a multifunctional NP[112]. The combination of NIR dye and drugs (theragnostic) for real-time monitoring of NPs utilizing NIR fluorescent within the in vivo imaging system (IVIS) in an orthotopic ovarian tumor model was thoroughly studied. A common knowledge that the peptide-HA NP is used as a diagnostic tool for ovarian cancer led to the development of ICG packed into self-assembled hyaluronic acid-based nanoparticles modified with different hydrophobic moieties and encapsulated into HA micelles specific for CD 44 and subsequently utilized in NIRF imaging. Safely concluding that HA micelles possess theragnostic potentials.

Nanobodies have been utilized as molecular imaging probes and therapeutic agents (theragnostics), especially those targeting cancer-specific membrane proteins. A future of noninvasive biopsies using PET, SPECT, MRI, OI, and nanobody-based tracers can be implemented. The cancer-specificity of NIR-labeled nanobodies visualizes the tumors (diagnosis) and assists the surgeon in complete tumor margin negative resections (therapy).

The prototype for theragnostics an SD-OCT-guided laser ablation system for brain tumor resections combines a scanning platform, OCT imaging, and laser ablation to deliver precise diagnosis and therapy in neurosurgery.[113]

E. Discussion

E1. General

The development and evolution of advanced nanotechnology can usher us into a new era of 21st-century precision medicine. Functional NPs for MRI need to be optimized and made available on a large scale and affordable cost together with high relaxivity, good biocompatibility, and biodegradability to translate into clinical applications. Despite the immense upside and great potential of NP, systems challenges exist. Firstly, toxicity is the main concern so more tests should be carried out and biocompatibility should be determined before human trials. Secondly, the issue of potency should be validated to determine the number of agents that are taken up in the target. Thirdly, the pharmacokinetics, the biodistribution, and the excretion of the NPs are interconnected to their shape, size, and surface status so vigorous studies should be undertaken to determine the stability of their delivery vehicles, their form, and size. Fourthly, the issue of targeting specificity should be addressed through studies that emphasize the specific interactions between MRI contrast agents' performance and EPR effect to establish a clinical valuable and specific strategy to obtain high-relaxivity NPs with strong EPR effect and optimal renal excretion. Lastly, the feasibility of this endeavor should be taken into consideration. NP-based MRI contrast agents should bring bench-top developed agents into the clinical application through a multidisciplinary approach. [114,4]

In an attempt to minimize toxicity biocompatible nanomaterials are used to coat or encapsulate magnetic moieties and bring T1 or T2 nanoparticle-based MRI contrast agents to clinical applications. Micelles have been employed and approved by the FDA for the aforementioned goal. Activatable MRI nanoprobes will play a critical role in the attempt to increase the specificity and sensitivity of T1 or T2 nanoparticle-based MRI CAs.[114]

Real-time IGS and synergistic anti-cancer strategies are the cornerstones of future applications in surgery, nanotechnology, and material science. The goal in any oncologic procedure is complete resection, negative boundaries, and elimination of micrometastasis which has produced underwhelming results through conventional surgery. A challenge that real-time IGS has shown great potential in overcoming and excel but first needs to find a way to decrease the cost of equipment, the radiation, and the high demands in the operation room.[4] Concluding, contrast agents that are currently employed for the aforementioned target display contradictory features such as enough surgical time window vs clearance time, in organic materials low quantum yield vs safety, and most importantly targeting specificity vs range of clinical applications. [4]

E2. Future perspectives

In NP-based MRI contrast agents, one of the holy grails in their development is tumor-specific agents. Studies have been undergone using metalloporphyrins which are selectively retained by a variety of tumors. Tumor-specific monoclonal antibody-labeled agents displayed enhancement in tumors, infection sites, and infarction sites. Ultra-high field MRI constitutes the future of MRI scanners offering enormous opportunities in biomedical science and clinical applications. However the contrast agents currently available cant operate in such high magnetic fields so in an attempt to overcome the challenge presented researchers used Dysprosium (Dy3+) and holmium (Ho3+) which due to their relatively short electronic relaxation time and sizeable magnetic moment demonstrated promising results.[59] Van Veggle and co-workers studied the size-dependent properties of NaDyF4 NPs under ultra-high magnetic fields and observed enhancement in T2-weighted MRI with increasing NP size and magnetic field strength. Theories that should be taken into great consideration have been recently developed regarding the use of NP as high-performance MRI CAs. Firstly, the size-dependent magnetization of magnetic NPs can be used to develop T2 CAs with high r2 values, and to generate T1 contrast with any given NP, the size effect of NPs will determine whether surface-to-volume ratio or tR is the dominant contributing factor. Secondly, the magnetic field inhomogeneity increased by shape anisotropy of magnetic NPs can be artificially regulated to enhance T2 relaxivity by reducing the symmetry of the induced field. Thirdly, engineering NPs as high-performance imaging agents should take into consideration their pharmacokinetics, metabolism, biodistribution, and surface modification. Ultra-small-sized NPs with higher relaxivity show promising results in this effect. Fourthly, precise cancer theragnostics utilizing NPs for stimuli-responsive MRI can be achieved by exploiting the microenvironment of tumors. Lastly, active molecular targeting via surface modification of QD can revolutionize the diagnosis and treatment of breast cancer. NIR-QD for intraoperative imaging and SLN mapping seems like an effective alternative to current methods.[114] Molecular imaging can achieve real-time intraoperative imaging with relatively high specificity, sensitivity, and resolution. Furthermore, molecular imaging can provide the precise detection of surgical

boundaries during surgery and increase tissue penetration by introducing new CAs for NIR-II and PA imaging. In conclusion, nanoprobes due to their relatively long retention time for sufficient operation windows with high quantum yields possess a great upside for image-guided surgery.[115]

F. Conclusion

This thesis aimed to provide an overview of functional nanoparticles for MRI and image-guided surgery. Nanoparticles-based MRI contrast agents have a prominent role in enhancing MRI sensitivity as T1, T2 – weighted imaging, and CEST contrast. Their facile surface modification through a high surface-to-volume ratio is discussed, along with other surface modification methods and core improvement. The recent development of paramagnetic and supermagnetic liposomes as versatile MRI probes are examined. Juxtaposed with always ''on'' MRI contrast agents, the emerging class of activatable MRI contrast agents with enhanced specificity and sensitivity due to their activation by specific stimuli combined with the benefits of nanomaterials can generate higher relaxivities and make them increasingly more attractive. This work also looked at the enhanced accumulation of nanoparticles at surgical sites and their contribution to image-guided surgery, synergistic strategies for precision surgery, and the elimination of tumors via real-time image-guided surgery.

Furthermore, nanotheranostics can revolutionize personalized medicine and are currently far from being fully exploited. Theranostic NPs hold great potential for improving various treatment strategies, among them therapeutic decision-making. The proper treatment strategy adjustment is crucial for the patient treatment success. Nanotechnology breaks new ground for cancer theranostics, and it may become another technological innovation in oncological surgery after minimally invasive technology with laparoscopic and robotic surgery. As we further learn about pathophysiology, biological behavior, and microenvironment characteristics of different types of cancers and physicochemical properties of NPs, as well as their connections, we are also learning about the most desirable NPs for IGS in the clinic.

G. References

1. Dale BM, Brown MA, Semelka RC, Brown MA. *MRI: Basic Principles and Applications*. Fifth edition. John Wiley & Sons, Ltd; 2015.

2. Tang H, Wu EX, Ma QY, Gallagher D, Perera GM, Zhuang T. MRI brain image segmentation by multi-resolution edge detection and region selection. *Computerized Medical Imaging and Graphics*. 2000;24(6):349-357. doi:10.1016/S0895-6111(00)00037-9

3. Mao X, Xu J, Cui H. Functional nanoparticles for magnetic resonance imaging. *WIREs Nanomed Nanobiotechnol*. 2016;8(6):814-841. doi:10.1002/wnan.1400

4. Wang C, Fan W, Zhang Z, Wen Y, Xiong L, Chen X. Advanced Nanotechnology Leading the Way to Multimodal Imaging-Guided Precision Surgical Therapy. *Adv Mater*. 2019;31(49):1904329. doi:10.1002/adma.201904329

5. Gao M, Yu F, Lv C, Choo J, Chen L. Fluorescent chemical probes for accurate tumor diagnosis and targeting therapy. *Chem Soc Rev*. 2017;46(8):2237-2271. doi:10.1039/C6CS00908E

6. Barreto JA, O'Malley W, Kubeil M, Graham B, Stephan H, Spiccia L. Nanomaterials: Applications in Cancer Imaging and Therapy. *Adv Mater*. 2011;23(12):H18-H40. doi:10.1002/adma.201100140

7. Michalet X, Pinaud FF, Bentolila LA, et al. Quantum Dots for Live Cells, in Vivo Imaging, and Diagnostics. *Science*. 2005;307(5709):538-544. doi:10.1126/science.1104274

8. Peer D, Karp JM, Hong S, Farokhzad OC, Margalit R, Langer R. Nanocarriers as an emerging platform for cancer therapy. *Nature Nanotech*. 2007;2(12):751-760. doi:10.1038/nnano.2007.387

9. Matsumura Y, Maeda H. A new concept for macromolecular therapeutics in cancer chemotherapy: mechanism of tumoritropic accumulation of proteins and the antitumor agent smancs. *Cancer Res*. 1986;46(12 Pt 1):6387-6392.

10. Li M, Zhang W, Wang B, Gao Y, Song Z, Zheng QC. Ligand-based targeted therapy: a novel strategy for hepatocellular carcinoma. *IJN*. 2016;Volume 11:5645-5669. doi:10.2147/IJN.S115727

11. Jain RK, Stylianopoulos T. Delivering nanomedicine to solid tumors. *Nat Rev Clin Oncol*. 2010;7(11):653-664. doi:10.1038/nrclinonc.2010.139

12. Golombek SK, May JN, Theek B, et al. Tumor targeting via EPR: Strategies to enhance patient responses. *Advanced Drug Delivery Reviews*. 2018;130:17-38. doi:10.1016/j.addr.2018.07.007

13. Cheng YH, He C, Riviere JE, Monteiro-Riviere NA, Lin Z. Meta-Analysis of Nanoparticle Delivery to Tumors Using a Physiologically Based Pharmacokinetic

Modeling and Simulation Approach. *ACS Nano*. 2020;14(3):3075-3095. doi:10.1021/acsnano.9b08142

14. Kaminskas LM, McLeod VM, Ryan GM, et al. Pulmonary administration of a doxorubicin-conjugated dendrimer enhances drug exposure to lung metastases and improves cancer therapy. *Journal of Controlled Release*. 2014;183:18-26. doi:10.1016/j.jconrel.2014.03.012

15. Li M, Gao Y, Yuan Y, et al. One-Step Formulation of Targeted Aggregation-Induced Emission Dots for Image-Guided Photodynamic Therapy of Cholangiocarcinoma. *ACS Nano*. 2017;11(4):3922-3932. doi:10.1021/acsnano.7b00312

16. Gao Y, Zheng QC, Xu S, et al. Theranostic Nanodots with Aggregation-Induced Emission Characteristic for Targeted and Image-Guided Photodynamic Therapy of Hepatocellular Carcinoma. *Theranostics*. 2019;9(5):1264-1279. doi:10.7150/thno.29101

17. Wang D, Lee MMS, Xu W, et al. Boosting Non-Radiative Decay to Do Useful Work: Development of a Multi-Modality Theranostic System from an AIEgen. *Angew Chem Int Ed*. 2019;58(17):5628-5632. doi:10.1002/anie.201900366

18. Wang P, Fan Y, Lu L, et al. NIR-II nanoprobes in-vivo assembly to improve image-guided surgery for metastatic ovarian cancer. *Nat Commun*. 2018;9(1):2898. doi:10.1038/s41467-018-05113-8

19. Ni X, Zhang X, Duan X, Zheng HL, Xue XS, Ding D. Near-Infrared Afterglow Luminescent Aggregation-Induced Emission Dots with Ultrahigh Tumor-to-Liver Signal Ratio for Promoted Image-Guided Cancer Surgery. *Nano Lett*. 2019;19(1):318-330. doi:10.1021/acs.nanolett.8b03936

20. Cao Y, Xu L, Kuang Y, Xiong D, Pei R. Gadolinium-based nanoscale MRI contrast agents for tumor imaging. *J Mater Chem B*. 2017;5(19):3431-3461. doi:10.1039/C7TB00382J

21. Louie A. Multimodality Imaging Probes: Design and Challenges. *Chem Rev*. 2010;110(5):3146-3195. doi:10.1021/cr9003538

22. Ratzinger G, Agrawal P, Körner W, et al. Surface modification of PLGA nanospheres with Gd-DTPA and Gd-DOTA for high-relaxivity MRI contrast agents. *Biomaterials*. 2010;31(33):8716-8723. doi:10.1016/j.biomaterials.2010.07.095

23. Zhu D, Liu F, Ma L, Liu D, Wang Z. Nanoparticle-Based Systems for T1-Weighted Magnetic Resonance Imaging Contrast Agents. *IJMS*. 2013;14(5):10591-10607. doi:10.3390/ijms140510591

24. Kukowska-Latallo J. Targeted gadolinium-loaded dendrimer nanoparticles for tumor-specific magnetic resonance contrast enhancement. *IJN*. Published online June 2008:201. doi:10.2147/IJN.S2696

25. Louie A. Multimodality Imaging Probes: Design and Challenges. *Chem Rev*. 2010;110(5):3146-3195. doi:10.1021/cr9003538

26. Rowe MD, Thamm DH, Kraft SL, Boyes SG. Polymer-Modified Gadolinium Metal-Organic Framework Nanoparticles Used as Multifunctional Nanomedicines for the Targeted Imaging and Treatment of Cancer. *Biomacromolecules*. 2009;10(4):983-993. doi:10.1021/bm900043e

27. Yim H, Yang SG, Jeon YS, et al. The performance of gadolinium diethylene triamine pentaacetate-pullulan hepatocyte-specific T1 contrast agent for MRI. *Biomaterials*. 2011;32(22):5187-5194. doi:10.1016/j.biomaterials.2011.03.069

28. Chen KJ, Wolahan SM, Wang H, et al. A small MRI contrast agent library of gadolinium(III)-encapsulated supramolecular nanoparticles for improved relaxivity and sensitivity. *Biomaterials*. 2011;32(8):2160-2165. doi:10.1016/j.biomaterials.2010.11.043

29. Liu Y, Chen Z, Liu C, Yu D, Lu Z, Zhang N. Gadolinium-loaded polymeric nanoparticles modified with Anti-VEGF as multifunctional MRI contrast agents for the diagnosis of liver cancer. *Biomaterials*. 2011;32(22):5167-5176. doi:10.1016/j.biomaterials.2011.03.077

30. Cheng Z, Thorek DLJ, Tsourkas A. Gadolinium-Conjugated Dendrimer Nanoclusters as a Tumor-Targeted T_1 Magnetic Resonance Imaging Contrast Agent. *Angew Chem Int Ed*. 2010;49(2):346-350. doi:10.1002/anie.200905133

31. Kumar R, Ohulchanskyy TY, Turowski SG, Thompson ME, Seshadri M, Prasad PN. Combined magnetic resonance and optical imaging of head and neck tumor xenografts using Gadolinium-labelled phosphorescent polymeric nanomicelles. *Head Neck Oncol*. 2010;2(1):35. doi:10.1186/1758-3284-2-35

32. Huang CH, Nwe K, Al Zaki A, Brechbiel MW, Tsourkas A. Biodegradable Polydisulfide Dendrimer Nanoclusters as MRI Contrast Agents. *ACS Nano*. 2012;6(11):9416-9424. doi:10.1021/nn304160p

33. Ladd DL, Hollister R, Peng X, et al. Polymeric Gadolinium Chelate Magnetic Resonance Imaging Contrast Agents: Design, Synthesis, and Properties. *Bioconjugate Chem*. 1999;10(3):361-370. doi:10.1021/bc980086+

34. Le UM, Cui Z. Long-circulating gadolinium-encapsulated liposomes for potential application in tumor neutron capture therapy. *International Journal of Pharmaceutics*. 2006;312(1-2):105-112. doi:10.1016/j.ijpharm.2006.01.002

35. Huang CH, Nwe K, Al Zaki A, Brechbiel MW, Tsourkas A. Biodegradable Polydisulfide Dendrimer Nanoclusters as MRI Contrast Agents. *ACS Nano*. 2012;6(11):9416-9424. doi:10.1021/nn304160p

36. Le UM, Cui Z. Long-circulating gadolinium-encapsulated liposomes for potential application in tumor neutron capture therapy. *International Journal of Pharmaceutics*. 2006;312(1-2):105-112. doi:10.1016/j.ijpharm.2006.01.002

37. Ni X, Zhang X, Duan X, Zheng HL, Xue XS, Ding D. Near-Infrared Afterglow Luminescent Aggregation-Induced Emission Dots with Ultrahigh Tumor-to-Liver Signal Ratio for Promoted Image-Guided Cancer Surgery. *Nano Lett*. 2019;19(1):318-330. doi:10.1021/acs.nanolett.8b03936

38. Li M, Gao Y, Yuan Y, et al. One-Step Formulation of Targeted Aggregation-Induced Emission Dots for Image-Guided Photodynamic Therapy of Cholangiocarcinoma. *ACS Nano*. 2017;11(4):3922-3932. doi:10.1021/acsnano.7b00312

39. Wang D, Lee MMS, Xu W, et al. Boosting Non-Radiative Decay to Do Useful Work: Development of a Multi-Modality Theranostic System from an AIEgen. *Angew Chem Int Ed*. 2019;58(17):5628-5632. doi:10.1002/anie.201900366

40. Wang P, Fan Y, Lu L, et al. NIR-II nanoprobes in-vivo assembly to improve image-guided surgery for metastatic ovarian cancer. *Nat Commun*. 2018;9(1):2898. doi:10.1038/s41467-018-05113-8

41. Maiseyeu A, Mihai G, Kampfrath T, et al. Gadolinium-containing phosphatidylserine liposomes for molecular imaging of atherosclerosis. *Journal of Lipid Research*. 2009;50(11):2157-2163. doi:10.1194/jlr.M800405-JLR200

42. Bridot JL, Faure AC, Laurent S, et al. Hybrid Gadolinium Oxide Nanoparticles: Multimodal Contrast Agents for in Vivo Imaging. *J Am Chem Soc*. 2007;129(16):5076-5084. doi:10.1021/ja068356j

43. Park JY, Baek MJ, Choi ES, et al. Paramagnetic Ultrasmall Gadolinium Oxide Nanoparticles as Advanced T_1 MRI Contrast Agent: Account for Large Longitudinal Relaxivity, Optimal Particle Diameter, and *In Vivo* T_1 MR Images. *ACS Nano*. 2009;3(11):3663-3669. doi:10.1021/nn900761s

44. Faucher L, Gossuin Y, Hocq A, Fortin MA. Impact of agglomeration on the relaxometric properties of paramagnetic ultra-small gadolinium oxide nanoparticles. *Nanotechnology*. 2011;22(29):295103. doi:10.1088/0957-4484/22/29/295103

45. Ni K, Zhao Z, Zhang Z, et al. Geometrically confined ultrasmall gadolinium oxide nanoparticles boost the T_1 contrast ability. *Nanoscale*. 2016;8(6):3768-3774. doi:10.1039/C5NR08402D

46. Ryu J, Park HY, Kim K, et al. Facile Synthesis of Ultrasmall and Hexagonal $NaGdF_4$: Yb^{3+} , Er^{3+} Nanoparticles with Magnetic and Upconversion Imaging Properties. *J Phys Chem C*. 2010;114(49):21077-21082. doi:10.1021/jp107725r

47. Tian G, Gu Z, Liu X, et al. Facile Fabrication of Rare-Earth-Doped Gd_2O_3 Hollow Spheres with Upconversion Luminescence, Magnetic Resonance, and Drug Delivery Properties. *J Phys Chem C*. 2011;115(48):23790-23796. doi:10.1021/jp209055t

48. Johnson NJJ, Oakden W, Stanisz GJ, Scott Prosser R, van Veggel FCJM. Size-Tunable, Ultrasmall $NaGdF_4$ Nanoparticles: Insights into Their T_1 MRI Contrast Enhancement. *Chem Mater*. 2011;23(16):3714-3722. doi:10.1021/cm201297x

49. Jin X, Fang F, Liu J, et al. An ultrasmall and metabolizable PEGylated $NaGdF_4$:Dy nanoprobe for high-performance T_1 /T_2 -weighted MR and CT multimodal imaging. *Nanoscale*. 2015;7(38):15680-15688. doi:10.1039/C5NR04065E

50. Hou Y, Qiao R, Fang F, et al. $NaGdF_4$ Nanoparticle-Based Molecular Probes for Magnetic Resonance Imaging of Intraperitoneal Tumor Xenografts *in Vivo*. *ACS Nano*. 2013;7(1):330-338. doi:10.1021/nn304837c

51. Xing H, Zhang S, Bu W, et al. Ultrasmall NaGdF $_4$ Nanodots for Efficient MR Angiography and Atherosclerotic Plaque Imaging. *Adv Mater*. 2014;26(23):3867-3872. doi:10.1002/adma.201305222

52. Liu C, Gao Z, Zeng J, et al. Magnetic/Upconversion Fluorescent NaGdF $_4$:Yb,Er Nanoparticle-Based Dual-Modal Molecular Probes for Imaging Tiny Tumors *in Vivo*. *ACS Nano*. 2013;7(8):7227-7240. doi:10.1021/nn4030898

53. Ni D, Zhang J, Bu W, et al. Dual-Targeting Upconversion Nanoprobes across the Blood–Brain Barrier for Magnetic Resonance/Fluorescence Imaging of Intracranial Glioblastoma. *ACS Nano*. 2014;8(2):1231-1242. doi:10.1021/nn406197c

54. Ma D, Meng L, Chen Y, et al. NaGdF $_4$:Yb $^{3+}$/Er $^{3+}$@NaGdF $_4$:Nd $^{3+}$@Sodium-Gluconate: Multifunctional and Biocompatible Ultrasmall Core–Shell Nanohybrids for UCL/MR/CT Multimodal Imaging. *ACS Appl Mater Interfaces*. 2015;7(30):16257-16265. doi:10.1021/acsami.5b05194

55. Zhou J, Zhu X, Chen M, Sun Y, Li F. Water-stable NaLuF4-based upconversion nanophosphors with long-term validity for multimodal lymphatic imaging. *Biomaterials*. 2012;33(26):6201-6210. doi:10.1016/j.biomaterials.2012.05.036

56. Tang SH, Wang J, Yang CX, Dong LX, Kong D, Yan XP. Ultrasonic assisted preparation of lanthanide-oleate complexes for the synthesis of multifunctional monodisperse upconversion nanoparticles for multimodal imaging. *Nanoscale*. 2014;6(14):8037. doi:10.1039/c4nr00806e

57. Pereira MIA, Pereira G, Monteiro CAP, et al. Hydrophilic Quantum Dots Functionalized with Gd(III)-DO3A Monoamide Chelates as Bright and Effective T1-weighted Bimodal Nanoprobes. *Sci Rep*. 2019;9(1):2341. doi:10.1038/s41598-019-38772-8

58. McAdams SG, Lewis DJ, McNaughter PD, et al. High magnetic relaxivity in a fluorescent CdSe/CdS/ZnS quantum dot functionalized with MRI contrast molecules. *Chem Commun*. 2017;53(76):10500-10503. doi:10.1039/C7CC05537D

59. Mulder WJM, Koole R, Brandwijk RJ, et al. Quantum Dots with a Paramagnetic Coating as a Bimodal Molecular Imaging Probe. *Nano Lett*. 2006;6(1):1-6. doi:10.1021/nl051935m

60. van Tilborg GAF, Mulder WJM, Chin PTK, et al. Annexin A5-Conjugated Quantum Dots with a Paramagnetic Lipidic Coating for the Multimodal Detection of Apoptotic Cells. *Bioconjugate Chem*. 2006;17(4):865-868. doi:10.1021/bc0600463

61. Kateb B, Chiu K, Black KL, et al. Nanoplatforms for constructing new approaches to cancer treatment, imaging, and drug delivery: What should be the policy? *NeuroImage*. 2011;54:S106-S124. doi:10.1016/j.neuroimage.2010.01.105

62. Busquets MA, Estelrich J, Sánchez-Martín MJ. Nanoparticles in magnetic resonance imaging: from simple to dual contrast agents. *IJN*. Published online March 2015:1727. doi:10.2147/IJN.S76501

63. Pan D, Caruthers SD, Senpan A, Schmieder AH, Wickline SA, Lanza GM. Revisiting an old friend: manganese-based MRI contrast agents: Manganese MRI contrast agents. *WIREs Nanomed Nanobiotechnol*. 2011;3(2):162-173. doi:10.1002/wnan.116

64. Vymazal J, Bulte JWM, Frank JA, Chiro GD, Brooks RA. Frequency dependence of MR relaxation times I. Paramagnetic ions. *J Magn Reson Imaging*. 1993;3(4):637-640. doi:10.1002/jmri.1880030413

65. Zhu J, Gale EM, Atanasova I, Rietz TA, Caravan P. Hexameric Mn ^{II} Dendrimer as MRI Contrast Agent. *Chem Eur J*. 2014;20(44):14507-14513. doi:10.1002/chem.201403883

66. Michalet X, Pinaud FF, Bentolila LA, et al. Quantum Dots for Live Cells, in Vivo Imaging, and Diagnostics. *Science*. 2005;307(5709):538-544. doi:10.1126/science.1104274

67. Zeng L, Wu D, Zou R, Chen T, Zhang J, Wu A. Paramagnetic and Superparamagnetic Inorganic Nanoparticles for T1-Weighted Magnetic Resonance Imaging. *CMC*. 2018;25(25):2970-2986. doi:10.2174/0929867324666170314124616

68. Busquets MA, Estelrich J, Sánchez-Martín MJ. Nanoparticles in magnetic resonance imaging: from simple to dual contrast agents. *IJN*. Published online March 2015:1727. doi:10.2147/IJN.S76501

69. Kim T, Momin E, Choi J, et al. Mesoporous Silica-Coated Hollow Manganese Oxide Nanoparticles as Positive T_1 Contrast Agents for Labeling and MRI Tracking of Adipose-Derived Mesenchymal Stem Cells. *J Am Chem Soc*. 2011;133(9):2955-2961. doi:10.1021/ja1084095

70. Chen Y, Yin Q, Ji X, et al. Manganese oxide-based multifunctionalized mesoporous silica nanoparticles for pH-responsive MRI, ultrasonography and circumvention of MDR in cancer cells. *Biomaterials*. 2012;33(29):7126-7137. doi:10.1016/j.biomaterials.2012.06.059

71. Zhen Z, Xie J. Development of Manganese-Based Nanoparticles as Contrast Probes for Magnetic Resonance Imaging. *Theranostics*. 2012;2(1):45-54. doi:10.7150/thno.3448

72. Chen Y, Chen H, Zhang S, et al. Structure-property relationships in manganese oxide - mesoporous silica nanoparticles used for T1-weighted MRI and simultaneous anti-cancer drug delivery. *Biomaterials*. 2012;33(7):2388-2398. doi:10.1016/j.biomaterials.2011.11.086

73. McMahon MT, Bulte JWM. Two decades of dendrimers as versatile MRI agents: a tale with and without metals: Dendrimers as versatile MRI agents. *WIREs Nanomed Nanobiotechnol*. 2018;10(3):e1496. doi:10.1002/wnan.1496

74. Pellico J, Ellis CM, Davis JJ. Nanoparticle-Based Paramagnetic Contrast Agents for Magnetic Resonance Imaging. *Contrast Media & Molecular Imaging*. 2019;2019:1-13. doi:10.1155/2019/1845637

75. Briley-Saebo K, Yeang C, Witztum JL, Tsimikas S. Imaging of Oxidation-Specific Epitopes with Targeted Nanoparticles to Detect High-Risk Atherosclerotic Lesions:

Progress and Future Directions. *J of Cardiovasc Trans Res*. 2014;7(8):719-736. doi:10.1007/s12265-014-9590-4

76. Silva AC, Lee JH, Aoki I, Koretsky AP. Manganese-enhanced magnetic resonance imaging (MEMRI): methodological and practical considerations. *NMR Biomed*. 2004;17(8):532-543. doi:10.1002/nbm.945

77. Hu F, Zhao YS. Inorganic nanoparticle-based T1 and T1/T2 magnetic resonance contrast probes. *Nanoscale*. 2012;4(20):6235. doi:10.1039/c2nr31865b

78. Kim BH, Lee N, Kim H, et al. Large-Scale Synthesis of Uniform and Extremely Small-Sized Iron Oxide Nanoparticles for High-Resolution T_1 Magnetic Resonance Imaging Contrast Agents. *J Am Chem Soc*. 2011;133(32):12624-12631. doi:10.1021/ja203340u

79. Park J, An K, Hwang Y, et al. Ultra-large-scale syntheses of monodisperse nanocrystals. *Nature Mater*. 2004;3(12):891-895. doi:10.1038/nmat1251

80. Jun Y wook, Huh YM, Choi J sil, et al. Nanoscale Size Effect of Magnetic Nanocrystals and Their Utilization for Cancer Diagnosis via Magnetic Resonance Imaging. *J Am Chem Soc*. 2005;127(16):5732-5733. doi:10.1021/ja0422155

81. Sun S, Zeng H, Robinson DB, et al. Monodisperse MFe_2O_4 (M = Fe, Co, Mn) Nanoparticles. *J Am Chem Soc*. 2004;126(1):273-279. doi:10.1021/ja0380852

82. Xiao L, Li J, Brougham DF, et al. Water-Soluble Superparamagnetic Magnetite Nanoparticles with Biocompatible Coating for Enhanced Magnetic Resonance Imaging. *ACS Nano*. 2011;5(8):6315-6324. doi:10.1021/nn201348s

83. Taboada E, Rodríguez E, Roig A, Oró J, Roch A, Muller RN. Relaxometric and Magnetic Characterization of Ultrasmall Iron Oxide Nanoparticles with High Magnetization. Evaluation as Potential T_1 Magnetic Resonance Imaging Contrast Agents for Molecular Imaging. *Langmuir*. 2007;23(8):4583-4588. doi:10.1021/la063415s

84. Chan N, Laprise-Pelletier M, Chevallier P, Bianchi A, Fortin MA, Oh JK. Multidentate Block-Copolymer-Stabilized Ultrasmall Superparamagnetic Iron Oxide Nanoparticles with Enhanced Colloidal Stability for Magnetic Resonance Imaging. *Biomacromolecules*. 2014;15(6):2146-2156. doi:10.1021/bm500311k

85. Li P, Chevallier P, Ramrup P, et al. Mussel-Inspired Multidentate Block Copolymer to Stabilize Ultrasmall Superparamagnetic Fe_3O_4 for Magnetic Resonance Imaging Contrast Enhancement and Excellent Colloidal Stability. *Chem Mater*. 2015;27(20):7100-7109. doi:10.1021/acs.chemmater.5b03028

86. Hannecart A, Stanicki D, Vander Elst L, et al. Nano-thermometers with thermo-sensitive polymer grafted USPIOs behaving as positive contrast agents in low-field MRI. *Nanoscale*. 2015;7(8):3754-3767. doi:10.1039/C4NR07064J

87. Filippousi M, Angelakeris M, Katsikini M, et al. Surfactant Effects on the Structural and Magnetic Properties of Iron Oxide Nanoparticles. *J Phys Chem C*. 2014;118(29):16209-16217. doi:10.1021/jp5037266

88. Lam T, Pouliot P, Avti PK, Lesage F, Kakkar AK. Superparamagnetic iron oxide based nanoprobes for imaging and theranostics. *Advances in Colloid and Interface Science*. 2013;199-200:95-113. doi:10.1016/j.cis.2013.06.007

89. Shokrollahi H. Structure, synthetic methods, magnetic properties and biomedical applications of ferrofluids. *Materials Science and Engineering: C*. 2013;33(5):2476-2487. doi:10.1016/j.msec.2013.03.028

90. Geraldes CFGC, Laurent S. Classification and basic properties of contrast agents for magnetic resonance imaging. *Contrast Media Mol Imaging*. 2009;4(1):1-23. doi:10.1002/cmmi.265

91. Hu F, Joshi HM, Dravid VP, Meade TJ. High-performance nanostructured MR contrast probes. *Nanoscale*. 2010;2(10):1884. doi:10.1039/c0nr00173b

92. Morawski AM, Winter PM, Crowder KC, et al. Targeted nanoparticles for quantitative imaging of sparse molecular epitopes with MRI: Molecular Imaging of Cellular Tissue Factor. *Magn Reson Med*. 2004;51(3):480-486. doi:10.1002/mrm.20010

93. Mornet S, Vasseur S, Grasset F, Duguet E. Magnetic nanoparticle design for medical diagnosis and therapy. *J Mater Chem*. 2004;14(14):2161. doi:10.1039/b402025a

94. Gómez-González E, Caro C, Martínez-Gutiérrez D, García-Martín ML, Ocaña M, Becerro AI. Holmium phosphate nanoparticles as negative contrast agents for high-field magnetic resonance imaging: Synthesis, magnetic relaxivity study and in vivo evaluation. *Journal of Colloid and Interface Science*. 2021;587:131-140. doi:10.1016/j.jcis.2020.11.119

95. Das GK, Johnson NJJ, Cramen J, et al. NaDyF $_4$ Nanoparticles as T $_2$ Contrast Agents for Ultrahigh Field Magnetic Resonance Imaging. *J Phys Chem Lett*. 2012;3(4):524-529. doi:10.1021/jz201664h

96. Bulte JWM, Wu C, Brechbiel MW, et al. Dysprosium-DOTA-PAMAM Dendrimers as Macromolecular T2 Contrast Agents: Preparation and Relaxometry. *Investigative Radiology*. 1998;33(11):841-845. doi:10.1097/00004424-199811000-00008

97. Caravan P, Greenfield MT, Bulte JWM. Molecular factors that determine Curie spin relaxation in dysprosium complexes. *Magn Reson Med*. 2001;46(5):917-922. doi:10.1002/mrm.1277

98. Ni D, Bu W, Zhang S, et al. Single Ho $^{3+}$ -Doped Upconversion Nanoparticles for High-Performance T_2 -Weighted Brain Tumor Diagnosis and MR/UCL/CT Multimodal Imaging. *Adv Funct Mater*. 2014;24(42):6613-6620. doi:10.1002/adfm.201401609

99. Ni D, Zhang J, Bu W, et al. PEGylated NaHoF4 nanoparticles as contrast agents for both X-ray computed tomography and ultra-high field magnetic resonance imaging. *Biomaterials*. 2016;76:218-225. doi:10.1016/j.biomaterials.2015.10.063

100. Terreno E, Cabella C, Carrera C, et al. From Spherical to Osmotically Shrunken Paramagnetic Liposomes: An Improved Generation of LIPOCEST MRI Agents with Highly Shifted Water Protons. *Angew Chem Int Ed*. 2007;46(6):966-968. doi:10.1002/anie.200604027

101. Peng Q, Yuan Y, Zhang H, et al. ^{19} F CEST imaging probes for metal ion detection. *Org Biomol Chem*. 2017;15(30):6441-6446. doi:10.1039/C7OB01068K

102. Cakić N, Savić T, Stricker-Shaver J, et al. Paramagnetic lanthanide chelates for multicontrast MRI. *Chem Commun*. 2016;52(59):9224-9227. doi:10.1039/C6CC04011J

103. Khemtong C, Kessinger CW, Gao J. Polymeric nanomedicine for cancer MR imaging and drug delivery. *Chem Commun*. 2009;(24):3497. doi:10.1039/b821865j

104. Kim KS, Park W, Hu J, Bae YH, Na K. A cancer-recognizable MRI contrast agents using pH-responsive polymeric micelle. *Biomaterials*. 2014;35(1):337-343. doi:10.1016/j.biomaterials.2013.10.004

105. Shubayev VI, Pisanic TR, Jin S. Magnetic nanoparticles for theragnostics. *Advanced Drug Delivery Reviews*. 2009;61(6):467-477. doi:10.1016/j.addr.2009.03.007

106. Cunningham CH, Arai T, Yang PC, McConnell MV, Pauly JM, Conolly SM. Positive contrast magnetic resonance imaging of cells labeled with magnetic nanoparticles. *Magn Reson Med*. 2005;53(5):999-1005. doi:10.1002/mrm.20477

107. Huang J, Zhong X, Wang L, Yang L, Mao H. Improving the Magnetic Resonance Imaging Contrast and Detection Methods with Engineered Magnetic Nanoparticles. *Theranostics*. 2012;2(1):86-102. doi:10.7150/thno.4006

108. Zhu J, Zhou L, XingWu F. Tracking Neural Stem Cells in Patients with Brain Trauma. *N Engl J Med*. 2006;355(22):2376-2378. doi:10.1056/NEJMc055304

109. Wu W, He Q, Jiang C. Magnetic Iron Oxide Nanoparticles: Synthesis and Surface Functionalization Strategies. *Nanoscale Res Lett*. 2008;3(11):397. doi:10.1007/s11671-008-9174-9

110. Kut C, Chaichana KL, Xi J, et al. Detection of human brain cancer infiltration ex vivo and in vivo using quantitative optical coherence tomography. *Sci Transl Med*. 2015;7(292). doi:10.1126/scitranslmed.3010611

111. Yang Z, Tian R, Wu J, et al. Impact of Semiconducting Perylene Diimide Nanoparticle Size on Lymph Node Mapping and Cancer Imaging. *ACS Nano*. 2017;11(4):4247-4255. doi:10.1021/acsnano.7b01261

112. Burkhardt JD, Natale A. New Technologies in Atrial Fibrillation Ablation. *Circulation*. 2009;120(15):1533-1541. doi:10.1161/CIRCULATIONAHA.109.858233

113. Cialla-May D, Zheng XS, Weber K, Popp J. Recent progress in surface-enhanced Raman spectroscopy for biological and biomedical applications: from cells to clinics. *Chem Soc Rev*. 2017;46(13):3945-3961. doi:10.1039/C7CS00172J

114. Mao X, Xu J, Cui H. Functional nanoparticles for magnetic resonance imaging. *WIREs Nanomed Nanobiotechnol*. 2016;8(6):814-841. doi:10.1002/wnan.1400

115. Wang C, Fan W, Zhang Z, Wen Y, Xiong L, Chen X. Advanced Nanotechnology Leading the Way to Multimodal Imaging-Guided Precision Surgical Therapy. *Adv Mater*. 2019;31(49):1904329. doi:10.1002/adma.201904329